BULETINUL INSTITUTULUI POLITEHNIC DIN IAŞI

Volumul 62 (66)

Numărul 1

CONSTRUCŢII DE MAŞINI

2016 **Editura POLITEHNIUM**

BULETINUL INSTITUTULUI POLITEHNIC DIN IAŞI
PUBLISHED BY
"GHEORGHE ASACHI" TECHNICAL UNIVERSITY OF IAŞI
Editorial Office: Bd. D. Mangeron 63, 700050, Iaşi, ROMANIA
Tel. 40-232-278683; Fax: 40-232-237666; *e-mail*: polytech@mail.tuiasi.ro

Editorial Board

Scientific Board

BULETINUL INSTITUTULUI POLITEHNIC DIN IAŞI
BULLETIN OF THE POLYTECHNIC INSTITUTE OF IAŞI
Volumul 62 (66), Numărul 1 2016

CONSTRUCŢII DE MAŞINI

SUMAR

BULETINUL INSTITUTULUI POLITEHNIC DIN IAŞI
BULLETIN OF THE POLYTECHNIC INSTITUTE OF IAŞI
Volume 62 (66), Number 1 2016

MACHINE CONSTRUCTION

CONTENTS

BULETINUL INSTITUTULUI POLITEHNIC DIN IAŞI
Publicat de
Universitatea Tehnică „Gheorghe Asachi” din Iaşi
Volumul 62 (66), Numărul 1, 2016
Secţia
CONSTRUCŢII DE MAŞINI

EXPERIMENTAL ASPECTS IN TWO-PHASE JET IN INTERACTION WITH THE FLAME

BY

DRAGOŞ PAVEL[1] and ALEXANDRU CHISACOF[2,*]

[1]Police Academy “Alexandru Ioan Cuza”, Bucharest, Romania,
Faculty of Fire Engineering
[2]POLITEHNICA University of Bucharest, Romania,
Department of Thermodynamics Engineering,
Engines, Thermal and Refrigeration

Received: May 5, 2015
Accepted for publication: June 1, 2015

Abstract. During the experimental test made on two-phase free jet, the specialized data acquisition equipment for direct measurement and thermal camera were used. Therefore the temperature field values and spectrum were obtained using the two described methods. The interference at the jet-flame boundary and the extinguish process by the warm water is verified. The experimental data and images are displayed in the paper. The pre-heating of liquid water allows a dispersion of that in fine droplets which gives a short time of evaporation, so high heat absorption, that causes an efficient flame extinguish. Using the warm water and an adequate nozzle dimension, a small quantity of water is used, and the damages are reduced.

Keywords: mist jet; infrared image; droplet lifetime; flame extinguish.

1. Introduction

Starting with the eighties, including Montreal Protocol in 1987, researchers looked for clean methods to extinguish fires, as an alternative to

*Corresponding author; *e-mail*: achisacof@clicknet.ro

halons (polluting fire extinguishing agents). A lot of the researches nowadays seek on reducing the droplet size, increasing thus the heat transfer surface, that leads to a quicker fire cooling and suppression (Liu and Kim, 2000, 2001; Beihua and Guangxuan, 2009). Very modest attention was given by researchers at the influence of extinguishing agent temperature.

Concerning the domain of droplets size and its influence on the efficient fire suppression the studies done by (Andersson *et al.*, 1996; Santangelo and Tartarini, 2010; Kumari *et al.*, 2010; Chisacof *et al.*, 2009-2011), are relevant. The experimental tests start from the premise that the warm water evaporates quickly, and will cool the fire in a shorter time than cold water. As fire suppression takes place faster, the amount of water used will be less and therefore, the collateral damage will be reduced. If warm water temperature will be used, suppression will occur earlier in comparison to the cold water mist.

It is well known that surface tension and the dynamic viscosity of liquid water decrease with the temperature. For the jet fluid atomisation the surface tension play an essential role. Based on data of water obtained from international tables (IAPWS-IF97, 2008), the evolution of surface tension with the temperature is presented in the Fig. 1 (Popa *et al.*, 2012). Regarding this surface tension variation we can see that there is a visible change in the slope around the temperature of 35°C - 40°C. The regression functions of the two zones are presented in Fig. 1.

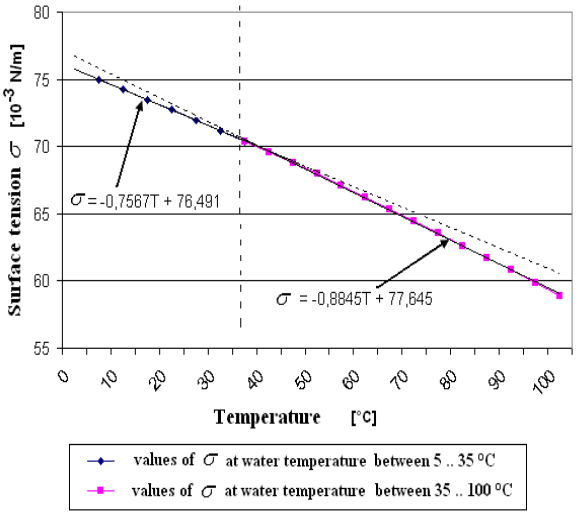

Fig. 1 − Surface tension of water versus temperature.

Other important parameters are the mean diameter range of the droplets and their lifetime in function of the liquid temperature. Fig. 2 presents the theoretical evaluation of these versus temperature (Pavel, 2009).

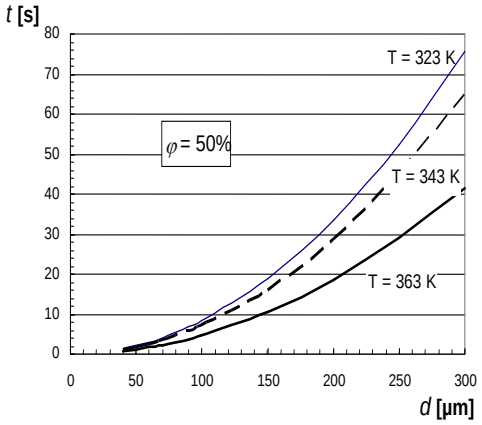

Fig. 2 − Life time versus size droplet at some temperatures.

Based on the above results, the authors chosen a range of temperatures that include the 30°C - 40°C interval. Water with these temperatures (13, 30 and 40°C), was used in different fire suppression tests, and the results were compared in order to obtain a domain which can be taken into account by designers for fixed water mist fire suppression systems.

2. Experimental Results

In aim to do the experimental tests we used the enhanced layout based on the experimental plant provided by (Pavel, 2009; Panaitescu *et al.*, 2012). The shape of the warm water spray realized by a 0.6 mm diameter nozzle and 30°C is presented on the Fig. 3. The abundance of wet vapour is observed in special at a height above 20 cm from the nozzle exit.

The temperature values from different heights and the distance from the nozzle axis is displayed on the Fig. 4. From this figure we examine the temperature field temperature on the jet envelope. Due to the variation of the emissivity factor in different jet vertical section the values must by corrected. Unfortunately the correction cannot be realized by the camera software and the information is only a qualitative one. Therefore, a direct contact measurement is recommended (Chisacof *et al.*, 2011)

The direct measurement of some points from the jet was made with thermocouples type K and the data acquisition system. From the Fig. 5, where the values were displayed, we note that the temperature in the same plane with the nozzle discharge becomes to have an important variation up to 25 cm around the jet axis (z = 0).

That means that suddenly, at the exit from the nozzle the evaporation of the warm liquid is important. The enlargement of the temperature field at this level may be due of the wet vapor generated at different heights. So, the liquid

density being higher than the air, the droplets fall due to gravitational field. From the Fig. 5 we observe for the heights above 25 cm the temperature variation becomes smaller, the difference being under 5 K.

Fig. 3 − Mist jet of warm water.

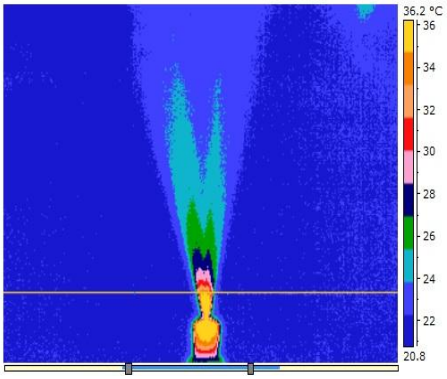

Fig. 4 − Infrared image of the warm mist jet.

This effect occurs due of the heat absorption from the surrounding, which has as the effect the jet cooling. Also, an enlargement of the variation temperature on the horizontal plane with the height is observed. From the Fig. 4 it is observed that the temperature falls in the first 50 cm from the exit nozzle.

Heat absorption potential of the jet, was evaluated using the experimental data at various inlet liquid temperatures for 0.6 mm nozzle diameter. In the analyzed case we present the droplet dispersion from a nozzle of 0.6 mm diameter for two temperatures 30°C. We observe that in the nozzle discharge plane the temperature becomes have an important variation from the 25 cm around the jet axis (z = 0). That means that suddenly, at the exit from the nozzle the evaporation of the warm liquid is important.

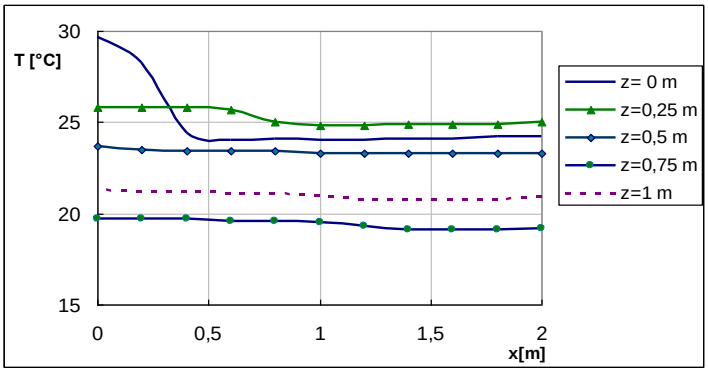

Fig. 5 − Temperature evolution in two phase jet (water inlet temperature 30°C).

The enlargement of the temperature field at this level may be due of the wet phase generated at different heights. So, the liquid density being higher than the air, the droplets fall due to gravitational field. From the same figure we observe for the heights above 25 cm the temperature variation becomes smaller, the difference being under 5 K.

The phenomena visualisation was made with the thermal camera HT 1016. The corresponding images are shown on the Fig. 6. From these images the infrared spectrum of temperature values is displayed on the right band. The flame core is reduced and the environmental temperature around 22°C is dominant (Fig. 6 *a*). The dark blue around the flame represents the water mist dispersed through a nozzle at 30°C. The incidence between the water mist and the flame has as result the flame reduction up to it is extinguished (Fig. 6 *a*). The same experience realised with the mist jet temperature of 13°C, shows us that the rate of flame reduction is lower than in the first case (Fig. 6 *b*). That is due the fact that the rate liquid evaporation is reduced, and consequently, the vapour concentration is weak and the oxygen molar fraction is beyond the low inflammability limit of the concerned fuel. Therefore the combustion time is greater than in the first case. Fig. 6 *c* shows the temperature at the boundary between the butane flame and the jet mist envelope. Due of the reduction of the oxygen concentration in the jet by water pre evaporation, combined with the heat absorption by the vaporized water, the flame cannot penetrate practically in the jet, only in a limited depth.

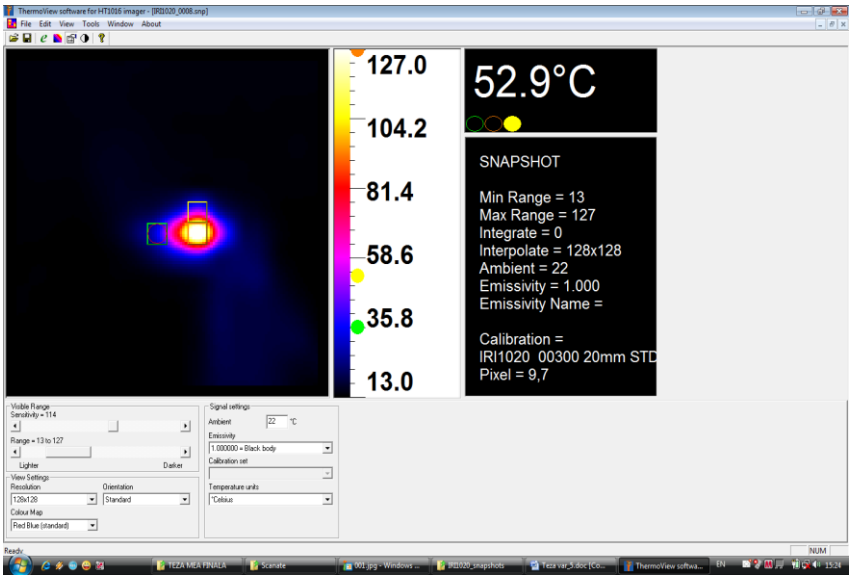

a

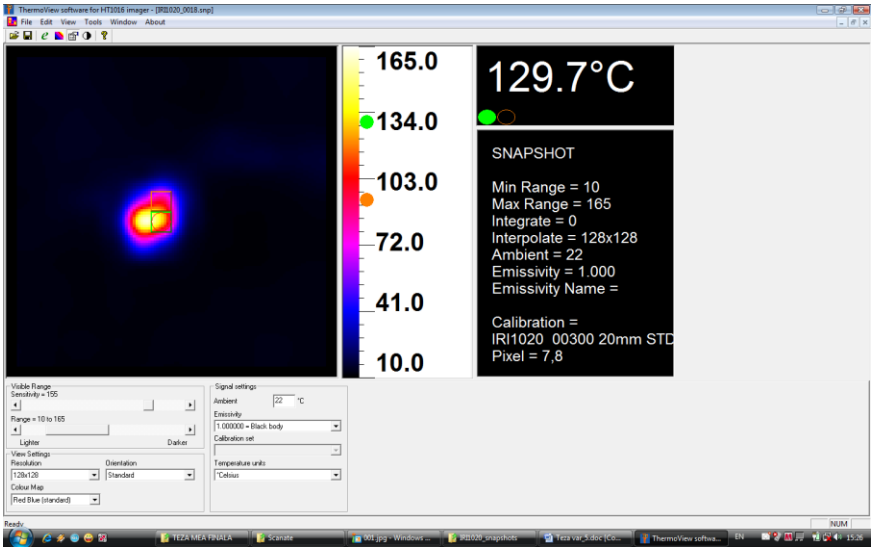

b

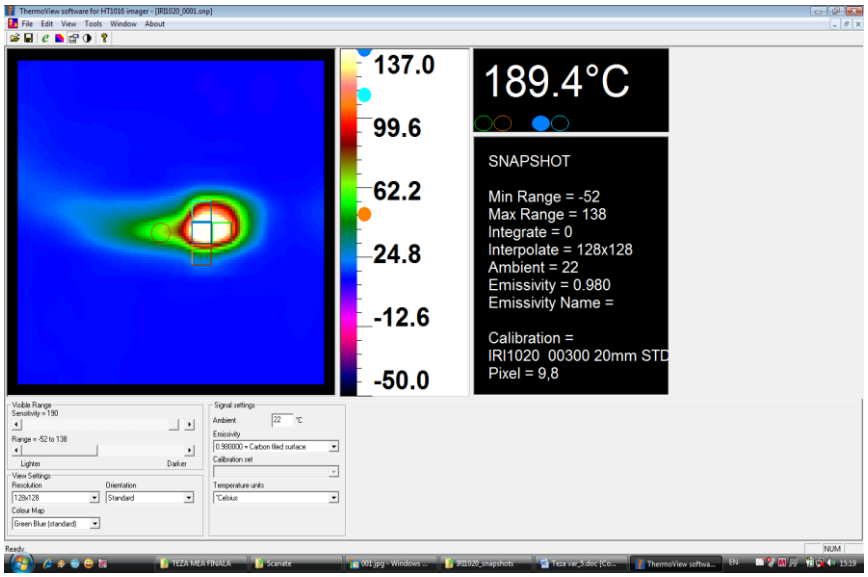

c

Fig. 6 − Infrared images at the mist jet – flame contact (thermal camera type HT 101).

Based on this observation we may conclude that the improvement of extinguish efficiency is realised with a warm jet mist, having at the nozzle exit

the temperature of 30°C. Our experiments show that in the butane case this temperature gives a shorter time extinguish interval. The explanation of this process is based on the fact that the pre evaporation fraction of liquid water is relatively reduced and the latent heat absorption by the flame is quiet sufficient for the flame extinguish. If the 13°C is used the initial evaporation is negligible.

In this sense must precise that thermophysical properties of water have an important role, especially the surface tension and the dynamic viscosity that decreases, which allows a shorter time of evaporation.

Our experiences with butane fuel gave the initial water temperature of 30°C as an appropriate one. The air concentration for the flame sustainability is in the range from 1.9-8.5% air fuel ratio (Sarlos *et al.*, 2003). By using the other fuels the mist temperature must be experienced.

3. Conclusions

1. The present study provides practical information concerning the liquid temperature influence of the jet dispersion and structure. The life time evolution of the droplets in function of the liquid temperature, diameters are shown. The case study analysis gives us the jet cone shape, its amplitude in function of the liquid temperature and the surrounding properties.

2. The experimental results illustrate that the warm liquid plays an important role in overall evaporation process: the droplet size and lifetime, jet boundary layer respectively. The measurement made in two modes, by direct contact and by infrared distance image capture are complementary, each of them giving the temperature values in the jet cone and on its boundary. The infrared pictures taken on the fire jet junction, allows us to evaluate the influence of the water temperature at nozzle exit. The impact of the water mist concerning the extinguish performance was applied on the butane flame.

3. The droplets distribution in the jet cone may furnish the place with the high values of heat absorption and consequently, the zone with an efficient fire extinguish. This fact generates a decrease of the temperature below the flame stability and an oxygen concentration reduction. Consequently, the flame failure may occur. The liquid rate for the extinguish process is reduced and the damages are limited.

REFERENCES

Andersson P., Arvidson M., Holmstedt G., *Small Scale Experiments and Theoretical Aspects of Flame Extinguishment with Water Mist*, Lund Institute of Technology, Lund University, Report 3080, May 1996.

Beihua C., Guangxuan L., *Experimental Studies on Water Mist Suppression of Liquid Fires with and without Additives*, Journal of Fire Sciences, **27**, *2*, 101−123, March 2009.

Chisacof A. *et al*., *Clean Jet for the Environment Structure Change,* Contract CNCSIS ID_1708/ 2009-2011.

Chisacof A., Panaitescu V., Pavel D., Poenaru M., *The Two Phase Jet Use in Semi-Open Space,* Proceedings of the ASME 2010 10th Biennial Conference on Engineering Systems Design and Analysis 2010, July 12-14, 2010, Istanbul, Turkey, paper ESDA2010-24961.

Chisacof A., Dimitriu S., Dragostin C., *Temperature Field from Free Two Phase Jet Using Infrared Equipment,* Conference METIME 2011, Galaţi-România, *3-4*, 5 p.

IAPWS-IF97, *International Association Properties of Water and Steam* (Editors Wagner W., Kretzschmar H.-J.), Springer Verlag, 2008.

Kumari N., Bahadur V., Hodes M., Salamon T., Kolodner P., Lyons A., Garimella S., *Analysis of Evaporating Mist Flow for Enhanced Convective Heat Transfer,* Raport, Birck and NCN Publications, 2010, 13 p.

Liu Z., Kim A.K. A *Review of Water Mist Fire Suppression Systems – Fundamental Studies,* Journal of Fire Protection Engineering, **10**, *3*, 32−50, 2000, 19 p.

Liu Z., Kim A.K., *A Review of Water Mist Fire Suppression Technology: Part II - Application Studies,* Journal of Fire Protection Engineering, **11**, *1*, 16−42, 2001.

Panaitescu V., Pavel D., Chisacof A., Lazaroiu G., *Free Jet of Mist Water Use for Fire Heat Absorption,* Revista de Chimie, **63**, *3*, 310−315, 2012.

Pavel D., Ph. D. Thesis, Politehnica University of Bucureşti, 2009.

Popa C., Chisacof A., Panaitescu V., *Experimental Clean Ethanol Pool Fire Suppression by Using Warm Water Mist,* Rev. Roum. Sci. Techn. – Électrotechn. et Énerg., **57**, *3*, 321–330, Bucureşti, 2012.

Santangelo P.E. Tartarini P., *Fire Control and Suppression by Water-Mist Systems,* The Open Thermodynamics Journal, **4**, 167−184, 2010, 18 p.

Sarlos G. *et al*., *Systèmes Energétiques* (*Energy Systems*), Editeur PPUR Presses Polytechniques, Suisse, 2003, 203-214.

ASPECTE EXPERIMENTALE ÎN JETURI BIFAZICE, ÎN INCIDENŢA CU FLACĂRA

(Rezumat)

Pe parcursul realizării experimentelor în jeturile bifazice s-au folosit aparate performante cu achiziţie de date, inclusiv o termocameră în infraroşu. Se obţin astfel, în spectrul infraroşu prin nuanţe de culori, gradienţii de temperatură, precum şi valorile aferente. Impactul între apa rece şi flacără, datorită duratei foarte scurte de interacţiune, nu permite evaporarea rapidă a lichidului, acesta fiind folosit în mică măsură, restul fiind pierdut. Din contra la injecţia apei preîncălzite, evaporarea este mult mai abundentă, iar stingerea flăcărilor de combustibil gazos devine mai eficientă. Prin folosirea apei calde şi a unui ajutaj de dispersie de dimensiuni adecvate, consumul de agent de stingere este redus, iar deteriorările colaterale se reduc.

BULETINUL INSTITUTULUI POLITEHNIC DIN IAŞI
Publicat de
Universitatea Tehnică „Gheorghe Asachi” din Iaşi
Volumul 62 (66), Numărul 1, 2016
Secţia
CONSTRUCŢII DE MAŞINI

EVALUATION OF UNDERGROUND SEASONAL SOLAR THERMAL ENERGY STORAGE

BY

ANDREI DUMENCU, GHEORGHE DUMITRAŞCU*, CONSTANTIN LUCA, IULIAN FILIP and BOGDAN HORBANIUC

"Gheorghe Asachi" Technical University of Iaşi, Romania,
Department of Mechanical Engineering

Received: April 24, 2015
Accepted for publication: October 8, 2015

Abstract. This paper presents an approximative analytical solution used to determine the heat seasonally stored underground. This model was applied for a period of 180 days, considering third kind of boundary conditions. The soil as an energy storage system, has always been considered to be a homogeneous environment with properties evaluated experimentally. The domain of thermal conductivity of soil, was approximately evaluated function of thermal conductivity of soil components. There were assumed two models in calculating the apparent thermal conductivity of the soil, serial and parallel. These models use the analogy between the thermal conductivity and electrical conductivity. The volume of each component depend on its concentration in soil. This approximate analytical solution can be adapted to actual soil composition, according to data collected through geological survey. Heat underground stored along the "warm" season, from spring to autumn, was calculated depending on the size of the underground heated volume function of the temperature field and apparent thermal conductivity.

Key words: thermal energy; energy storage; soil composition.

*Corresponding author; *e-mail*: gdum@mt.tuiasi.ro

1. Introduction

Storing underground solar thermal energy during "warm" season, might be a way to extend the operation of geothermal heat pump based systems during the winter.

It is very difficult to evaluate accurately the underground apparent thermal conductivity and thus the seasonal stored heat function on the evolution of temperature field in time and finally the energy efficiency of corresponding geothermal heat pump based systems during the winter. Therefore the evaluation of the costs/savings ratio is nearly impossible. Some studies proved that thermal conductivity of soil, is related to water content and bulk density (Evett *et al.*, 2012; Schibuola *et al.*, 2013). A higher water content in soil, causes an increase in thermal conductivity.

Other underground thermal energy storage systems, are using aquifer for storing heat (or cold) (Diersch and Bauer, 2015). In this case, an open loop heat pump is necessary, to extract water form a place in the ground and then inject it or evacuate it in another location. Usually, this type of heat pumps, are used for cooling buildings, like large university buildings in Turin, Italy (Lo Russo *et al.*, 2011), or for an IKEA store from Collegno, Italy (Lo Russo and Civita, 2009).

To improve underground thermal energy storage systems, R. Yumrutas and M. Unsal developed a model with an underground storage tank, that uses water to store thermal energy (Yumrutas and Unsal, 2012). This paper also presents soil as a homogeneous medium, made out of limestone, coarse or granite.

Also, as presented in the paper wrote by Zhang *et al*. (2007), one of the soil characteristics that causes errors between developed model and experimental data about thermal conductivity of soils, is quarts quantity in it, because quartz has a high thermal conductivity. In this paper is also presented a similar model developed by us, since they also consider soil to be formed by air, water and soil, but they used porosity, degree of saturation and effective thermal properties of the soil, dependent of type of soil.

Evaluating the amount of energy that can be stored in ground during a season, that is known also as a storage phase, could provide data for storage volume and land surface needed in order to store a certain amount of thermal energy and depth required in order to avoid influence of weather over the stored heat. Also an important role in storing thermal energy, is attributed to heat exchanger, borehole diameter, depth and grouting thermal conductivity, as proved by Luo *et al.* (2013).

In this paper we try to adapt an analytical solution for semi-infinite walls in order to approximately evaluate solar thermal energy that can be stored in ground during the warm season. Apparent thermal conductivity was calculated using electrical models of series and parallel. The real thermal conductivity is considered to be limited by those two apparent thermal conductivities evaluated by those two models.

2. Mathematical Model

2.1. Initial Data and Boundary Conditions

In this paper, ground is considered to be a semi-infinite plane wall, with a thermal conductivity calculated from all thermal conductivities of main substances that composes soil. For calculating average thermal conductivity of ground, we assume, from electrical theory, that particles are arranged in series and parallel, as seen in Fig. 1.

The small particles that compose soil, are noted in Table 1 with their dimensions (Ward Chesworth, 2008). We can assume that a bigger particle (with series and parallel arrangement) will contain all substances that are part of ground and for this particle is calculated the minimum and maximum thermal conductivity and heat capacity.

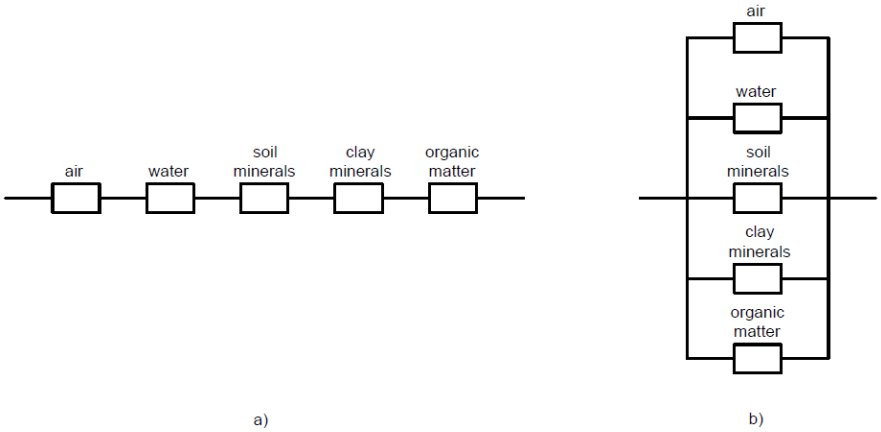

Fig. 1 – Soil particles arrangement for estimating average soil thermal conductivity: *a*) series arrangement; *b*) parallel arrangement.

Table 1

The Relative Sizes of Sand, Silt and Clay Particles (Taylor and Fancis, 2006)

Name	Size, diameter [mm]
Very coarse sand	1 – 2
Coarse sand	0.5 – 1
Medium sand	0.25 – 0.5
Fine sand	0.1 – 0.25
Very fine sand	0.05 – 0.1
Silt	0.002 – 0.05
Clay	Smaller than 0.002

Thermal properties of substances that form the ground are listed in the Table 2 (Blasch, 2003; Ward Chesworth, 2008).

Table 2
Thermal Properties of Substances that form Ground
(Blasch, 2003; Ward Chesworth, 2008)

Name	Density $10^6 gm^{-3}$	Volumetric thermal capacity $10^6 Jm^{-3}°C^{-1}$	Thermal conductivity $Wm^{-1}°C^{-1}$	Thermal diffusivity $10^{-6} m^2 s^{-1}$
Air	0.001	0.001	0.024	19
Liquid water	1.0	4.2	0.60	0.14
Ice	0.9	1.9	2.2	1.2
Quartz (Sand)	2.7	1.9	8.4	4.3
Sand minerals	2.7	1.9	2.9	1.5
Clay minerals	2.7	2.0	2.9	1.5
Organic matter	1.3	2.5	0.25	0.10

Particles considered in this model are air, liquid water, sand minerals, clay minerals and organic matter, with ratio of 25%, 25% 25%, 20% and respectively 5%.

The model used for developing this thermal storage evaluation is a beam, Fig. 2, that is 20 m in length and has a section area of 1x1 m.

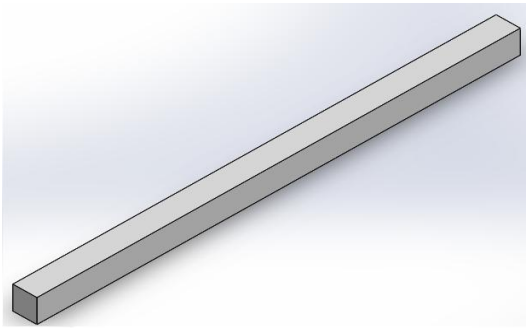

Fig. 2 – Design of soil for evaluating underground thermal storage.

2.2. Apparent Thermal Conductivity Evaluation

We consider soil to be a semi infinite wall, with a constant heat flux, and an equivalent thermal conductivity, calculated from thermal conductivities of particles that compose ground.

From electricity we know that average resistance for series mounting is:

$$R_s = \sum_{i=1}^{n} R_i \tag{1}$$

And for parallel mounting is:

$$R_p = \sum_{i=1}^{n} \frac{1}{R_i} \tag{2}$$

Thermal resistance is:

$$R_t = \frac{\delta_i}{k_i} \tag{3}$$

To evaluate proportions of each substance in soil, we will use an equivalent volumic concentration:

$$x_i = \frac{\delta_i}{\delta} \cdot \frac{A_i}{A} \tag{4}$$

where:

$$\delta = \delta_a + \delta_w + \delta_{sm} + \delta_{cm} + \delta_{om} \tag{5}$$

From Eqs. (1)-(4) we assume that equivalent thermal conductivity is:
− for series particles:

$$k_s = \frac{1}{\frac{x_a}{k_a} + \frac{x_w}{k_w} + \frac{x_{sm}}{k_{sm}} + \frac{x_{cm}}{k_{cm}} + \frac{x_{om}}{k_{om}}} \tag{6}$$

− for parallel particles:

$$k_p = k_a \cdot x_a + k_w \cdot x_w + k_{sm} \cdot x_{sm} + k_{cm} \cdot x_{cm} + k_{om} \cdot x_{om} \tag{7}$$

We assumed the third kind boundary conditions, respectively, constant mean temperature of heat transfer fluid and constant convective heat transfer coefficient.

During charge phase, we assume heat transfer from heat exchanger to be convective:

$$q(t) = h \cdot [T_0 - T(0,t)] \tag{8}$$

2.3. Mathematical Equation

Analytical equations of temperature field, from heat flux will be (Cengel and Gajar, 2015):

$$\frac{T(x,t)-T_0}{T_f-T_0}=erfc\left(\frac{x}{2\sqrt{\alpha\cdot t}}\right)-exp\left(\frac{h\cdot x}{k}+\frac{x^2\cdot\alpha\cdot t}{k^2}\right)\cdot erfc\left(\frac{x}{2\sqrt{\alpha\cdot t}}+\frac{h\sqrt{\alpha\cdot t}}{k}\right) \quad (9)$$

Heat accumulated underground during time *t*, is:

$$\delta Q_{ac}=A\cdot C_v\cdot\left[T(x,t_e)-T_0\right]dx \quad (10)$$

where

$$Q_{ac}=\int_0^x A\cdot C_v\cdot\left[T(x,t_e)-T_0\right]dx \quad (11)$$

2.4. Numerical Results

According to data from Tables 1 and 2, we can calculate next dimensions:
− gross dimension soil particle, containing all soil components, δ

$$\delta=(0.025+0.025+0.1+0.002+0.005)\cdot10^{-3}=0.157\cdot10^{-3}\text{m} \quad (12)$$

− equivalent thermal conductivity for particles arranged in series:

$$k_s=\frac{1}{\left(\frac{0.15926}{0.024}+\frac{0.15926}{0.6}+\frac{0.63694}{2.9}+\frac{0.01273}{2.9}+\frac{0.03184}{0.25}\right)\cdot10^{-3}}= \\ =0.1379\text{W}/(\text{K}\cdot\text{m}) \quad (13)$$

− equivalent thermal conductivity for particles arranged in parallel:

$$k_p=(0.024\cdot0.15926+0.6\cdot0.15926+2.9\cdot0.63694+2.9\cdot0.01273+ \\ +0.25\cdot0.03184)\cdot10^{-3}=1.99\text{W}/(\text{K}\cdot\text{m}) \quad (14)$$

Assuming that underground temperature is constant, at 10°C, so, T_0 = 10°C and considering heat pump to have an auxiliary heat storage system in order to keep the temperature of heat transfer fluid constant, at 30°C or higher, T_f = 30°C, during day and night and during cloudy days, we need to evaluate heat flux from heat exchanger to underground, using Eq. (9) and (15).

$$q=-k\cdot\left.\frac{\partial T}{\partial x}\right|_{x=0} \quad (15)$$

Heat flux according to time, was determined for a period of 1 h, 1 day, 10 days and 180 days. As we can see from Fig. 3, heat flux decreases quickly in 1st hour of charging and during 1 day is decreasing under 100 W/m^2. In this evaluation we used red line for series arrangement and blue line for parralel arrangement of soil composition.

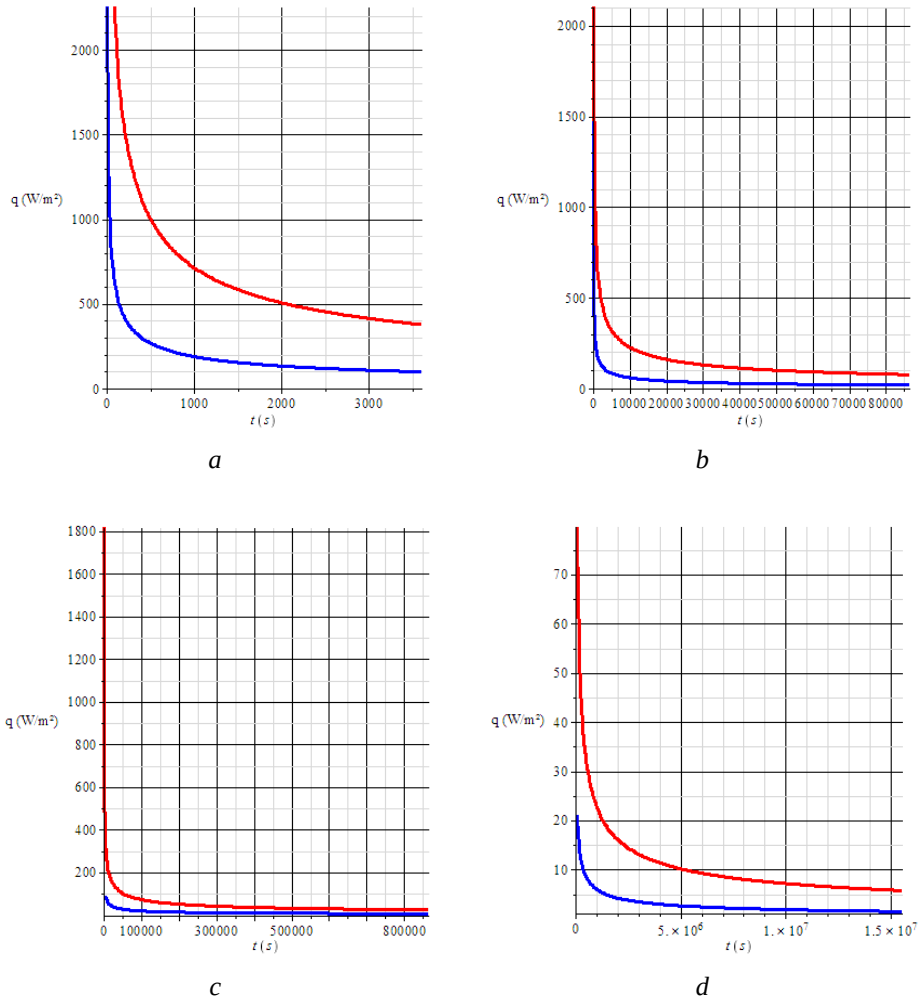

Fig. 3 – Heat flux during different time periods:
a) t = (0 .. 3600) s (1h); *b*) t = (0 .. 86400) s (1 day);
c) t = (0 .. 864000) s (10 days); *d*) t = (0 .. 15552000) s (180 days).

In Table 3 is presented heat flux for certain periods of time.

Table 3
Heat Flux Variation in Time

Heat flux q, [W/m^2]		Time of charging thermal energy undergound, [s]
series	parallel	
4444.5	7721.2	1 s
767.4	2644.3	60 s (1 min)
141.3	534.6	1800 s (30 min)
99.9	378.9	3600 s (1 h)
28.8	109.6	43200 s (12 h)
20.4	77.5	86400 s (1 day)
6.45	24.5	864000 s (10 days)
3.72	14.15	(30 days)
2.63	10	(60 days)
1.86	7.08	(120 days)
1.53	5.78	(180 days)

From Fig. 3, it can be observed that heat flux to charging face, is rapidly decreasing, due to the fact that temperature of heated face, increases by heat gained. A low thermal conductivity, causes heat to dissipate slow inside an semi-infinite soild, so while accumulated heat increases, heat flux decreases.

Assuming that, heat will be charged in ground for 180 days, 24 h each day.

$$t = 180\text{days} \cdot 24\text{h} \cdot 3600\text{s} = 1.5552 \cdot 10^7\,\text{s} \tag{16}$$

Density for gross particle that contains all ground compositions, will be calculated as a proportion of each one of the substances:

$$\rho = \rho_a \cdot 25\% + \rho_w \cdot 25\% + \rho_{sm} \cdot 25\% + \rho_{cm} \cdot 20\% + \rho_{om} \cdot 5\% \tag{17}$$

$$\begin{aligned} \rho &= \left(0.001 \cdot 25\% + 1 \cdot 25\% + 2.7 \cdot 25\% + 2.7 \cdot 20\% + 1.3 \cdot 5\%\right) \cdot 10^3 \\ &= 1.53 \cdot 10^3\,\text{kg/m}^3 \end{aligned} \tag{18}$$

Similar conditions are used to calculate volumetric thermal capacity for gross particle:

$$c_v = c_{va} \cdot 25\% + c_{vw} \cdot 25\% + c_{vsm} \cdot 25\% + c_{vcm} \cdot 20\% + c_{vom} \cdot 5\% \tag{19}$$

$$\begin{aligned} c_v &= (0.001 \cdot 25\% + 4.2 \cdot 25\% + 1.9 \cdot 25\% + 2 \cdot 20\% + 2.5 \cdot 5\%) \cdot 10^6 \\ &= 2.05 \cdot 10^6\,\text{J/(m}^3 \cdot \text{K)} \end{aligned} \tag{20}$$

Thermal diffusivity can now be calculated, for gross soil particle, for series and parallel arrangement with equation:

$$\alpha_{s,p} = \frac{k_{s,p}}{c_v} \tag{21}$$

− for series arrangement:

$$\alpha_s = \frac{0.1379}{2.05 \cdot 10^6} = 6.726 \cdot 10^{-8}\,\mathrm{m^2/s} \tag{22}$$

− for parallel arrangement:

$$\alpha_p = \frac{1.99}{2.05 \cdot 10^6} = 9.713 \cdot 10^{-7}\,\mathrm{m^2/s} \tag{23}$$

To find the interval of heat accumulated in ground, during time *t*, we solve Eq. (11) using (9) and get:

$$Q_{ac_{s,p}} = -\int_0^x \left[A \cdot c_v \cdot \left(T_0 - T_f\right) \left(erfc\left(\frac{x}{2\sqrt{t \cdot \alpha_{s,p}}} \right) - erfc\left(\frac{x}{2\sqrt{t \cdot \alpha_{s,p}}} + \frac{h\sqrt{t \cdot \alpha_{s,p}}}{k_{s,p}} \right) \cdot e^{\frac{h \cdot x}{k_{s,p}} + \frac{h^2 \cdot t \cdot \alpha_{s,p}}{k^2_{s,p}}} \right) \right] dx \tag{24}$$

Amount of heat that can be stored underground in one cubic meter of soil (A = 1 m^2, x = 1 m), considering temperature of fluid at 30°C, heat convection coefficient at 10 W(m^{2}K) and initial temperature in soil of 10°C, will be:

− for series arrangement:

$$Q_{ac_s} = 2.9837 \cdot 10^7\,\mathrm{J} = 29.8371\,\mathrm{MJ} \tag{25}$$

− for parallel arrangement:

$$Q_{ac_p} = 3.686 \cdot 10^7\,\mathrm{J} = 36.8635\,\mathrm{MJ} \tag{26}$$

Heat accumulated underground in 180 day, with heat transfer fluid at a temperature of 30°C, should vary between 29.8371 MJ and 36.8635 MJ. We calculated the amount of heat that will accumulate for both arrangements, so that we can have an interval to verify upcoming results.

For accurate results, we calculate different mean values, arithmetic (am), geometric (gm), harmonic (hm) and logarithmic (lg), of thermal conductivities between series and parallel arrangements of soil particles.

$$k_{am} = \frac{k_s + k_p}{2} = \frac{0.1379 + 1.99}{2} = 1.065 \mathrm{W/(m \cdot K)} \tag{27}$$

And thermal diffusivity for arithmetic mean of thermal conductivity:

$$\alpha_{am} = \frac{k_{am}}{c_v} = \frac{1.065}{2.05 \cdot 10^6} = 5.193 \cdot 10^{-7} \mathrm{m/s^2} \tag{28}$$

In this scenario, considering initial data the same, accumulated heat, is:

$$Q_{am} = 36.1 \mathrm{MJ} \tag{29}$$

For geometric mean:

$$k_{gm} = \sqrt{k_s \cdot k_p} = \sqrt{0.1379 \cdot 1.99} = 0.524 \mathrm{W/(m \cdot K)} \tag{30}$$

$$\alpha_{gm} = \frac{k_{gm}}{c_v} = \frac{0.524}{2.05 \cdot 10^6} = 2.556 \cdot 10^{-7} \mathrm{m^2/s} \tag{31}$$

$$Q_{ac_{gm}} = 34.66 \mathrm{MJ} \tag{32}$$

For harmonic mean:

$$k_{hm} = \frac{2}{\frac{1}{k_s} + \frac{1}{k_p}} = \frac{2}{\frac{1}{0.1379} + \frac{1}{1.99}} = 0.2579 \mathrm{W/(m \cdot K)} \tag{33}$$

$$\alpha_{hm} = \frac{k_{hm}}{c_v} = \frac{0.2579}{2.05 \cdot 10^6} = 1.258 \cdot 10^{-7} \mathrm{m^2/s} \tag{34}$$

$$Q_{ac_{hm}} = 32.50 \mathrm{MJ} \tag{35}$$

For logarithmic mean:

$$k_{\lg} = \frac{k_s - k_p}{\ln k_s - \ln k_p} = \frac{0.1379 - 1.99}{\ln(0.1379) - \ln(1.99)} = 0.6942 \text{W} / (\text{m} \cdot \text{K}) \tag{36}$$

$$\alpha_{\lg} = \frac{k_{\lg}}{c_v} = \frac{0.6942}{2.05 \cdot 10^6} = 3.386 \cdot 10^{-7} \text{m}^2 / \text{s} \tag{37}$$

$$Q_{ac_{\lg}} = 35.32 \text{MJ} \tag{38}$$

where: Qacs – heat accumulated using series arrangement of soil particles for calculating thermal conductivity; Qacp – heat accumulated using parallel arrangement of soil particles for calculating thermal conductivity; Qacam – heat accumulated using arithmetic mean between thermal conductivities of series and parallel arrangement; Qacgm – heat accumulated using geometric mean between thermal conductivities; Qachm – heat accumulated using harmonic mean between thermal conductivities; Qaclg – heat accumulated using logarithmic mean between thermal conductivities.

Ranging the distance *x*, from 0.01 m, to 20 m, we can observe how heat is accumulating underground in 180 days, from graph presented in Fig. 4. It can be observed that if heat transfer fluid has a steady temperature of 30°C, heat will only be stored in 10 m^3 of soil and after 10 m, soil will no longer store heat.

We used ANSYS to verify the results obtained and it proved that our results are confirmed, as seen in Fig. 5.

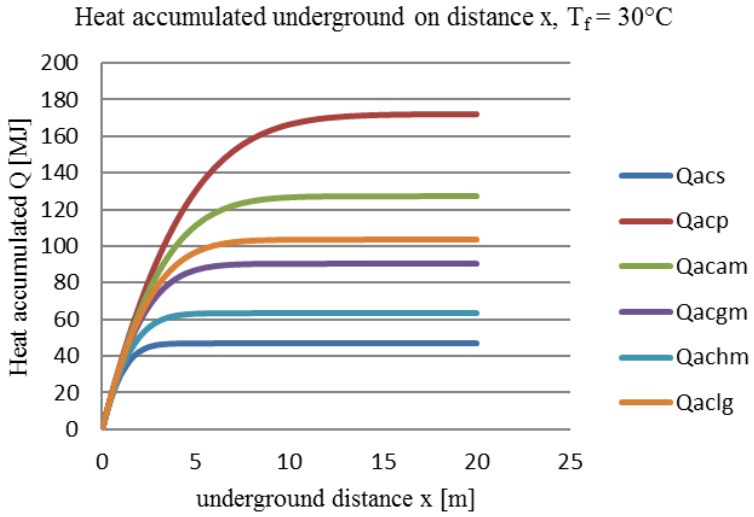

Fig. 4 – Heat accumulated underground using various methods to achieve a mean thermal conductivity for soil, using a constant temperature for heat transfer fluid of 30°C.

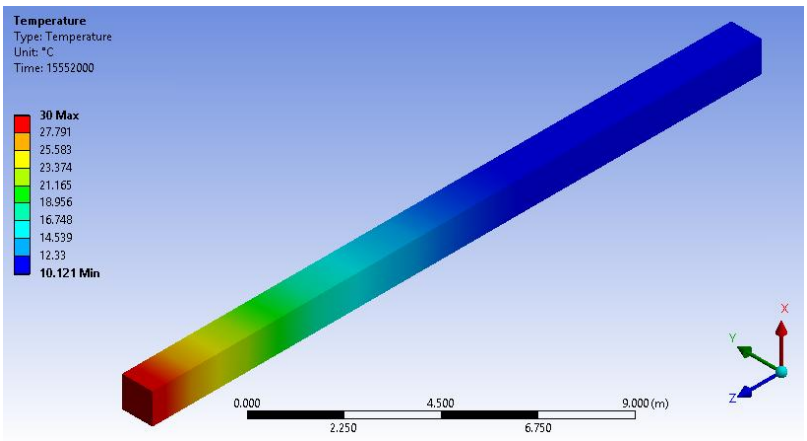

Fig. 5 – Heat accumulated underground using various methods to achieve a mean thermal conductivity for soil, using a constant temperature of heat transfer fluid of 30°C.

Another analisys was made with constant temperature of heat transfer fluid of 120°C. The graph presented in Fig. 6, was developed using equations above and it showed that the difference between temperature of heat transfer fluid from 30°C to 120°C is only in quantity of stored heat, in the same volume of soil. Again, results were verified with ANSYS and presented in Fig. 7.

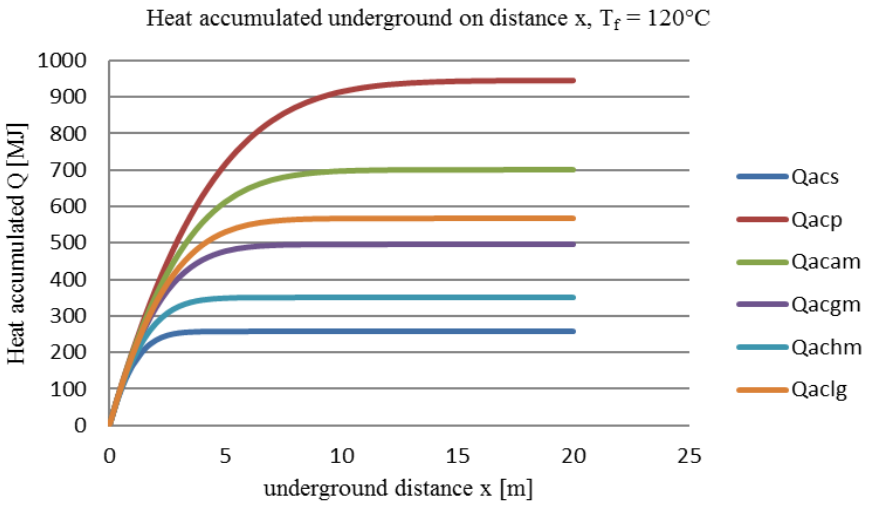

Fig. 6 – Heat accumulated underground using various methods to achieve a mean thermal conductivity for soil, using a constant temperature for heat transfer fluid of 120°C.

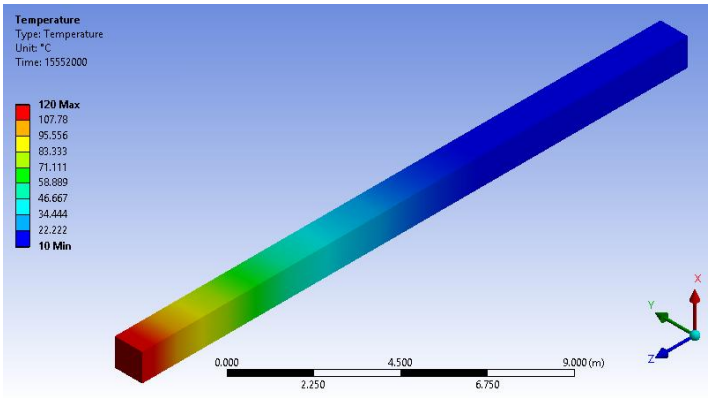

Fig. 7 – Heat accumulated underground using various methods to achieve a mean thermal conductivity for soil, using a constant temperature for heat transfer fluid of 120°C.

From graph in Figs. 4-7, we can see that Q_{ac}, accumulated heat, will increase slower after 10 m, because temperature inside soil increseas and storage volume remains almost constant. So we can consider a volume of 10 m^3 to 13 m^3 of soil to be enough for our underground energy storage, using this configuration.

In order to prove that by using a constant volume of soil, accumulated heat underground is increasing by increasing temperature of heat transfer fluid and also observe how thermal conductivity affects heat storage, in point x = 1 m, if we increase temperature of heat transfer fluid, from 30°C, to 120°C, we can see that accumulated heat will also increase, Fig. 8. We did the same, for x = 10 m, in this case, 10 m^3 of soil and presented results in Fig. 9.

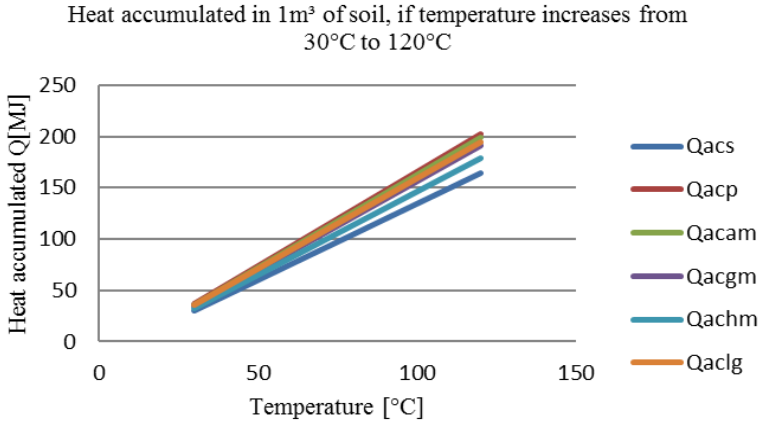

Fig. 8 – Heat accumulated underground if temperature of heat transfer fluid would increase from 30°C to 120°C.

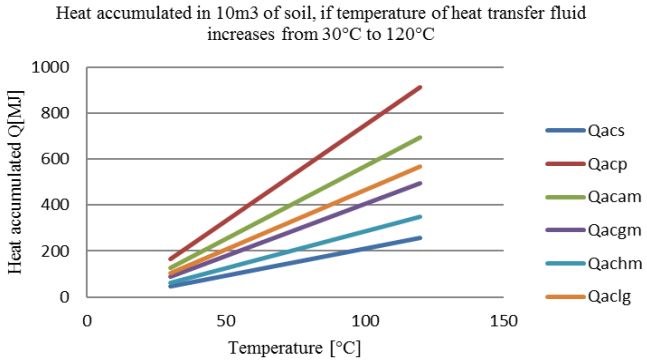

Fig. 9 – Heat accumulated underground if temperature of heat transfer fluid would increase from 30°C to 120°C.

From all graphs, we can see that a higher thermal conductivity of soil, will increase accumultated heat underground, but also, will increase the volume soil needed for heat storage.

It can be observed from Fig. 9, that in 180 days of charing thermal energy underground, in 10 m^3 of soil, thermal conductivity of soil has a serious impact over accumulated heat. For a temperature of heat transfer fluid of 120°C and a thermal conductivity of 0.1379 W/(m·K), in case of series arrangement of soil particles, accumulated heat in 180 days, is 257.18 MJ. In same conditions, accumultated heat for a thermal conductivity of 1.99 W/(m·K), is 914.60 MJ. So a soil rich in clay minerals and sand minerals is preffered in order to store thermal energy.

In Fig. 10, is presented heat accumulated varying time, using temperature of heat transfer fluid of 30°C.

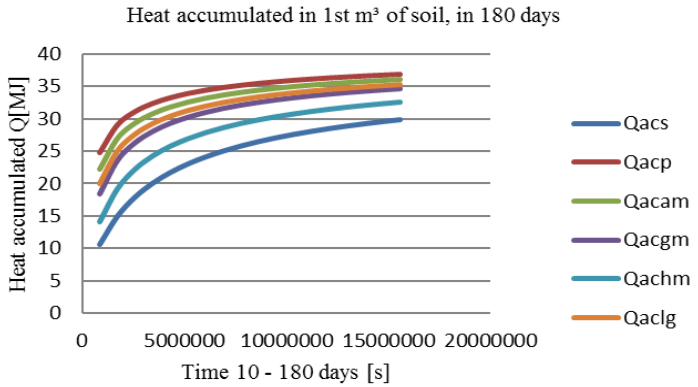

Fig. 10 – Heat accumulated underground for x = 1, (1 m^3), in time, from day 10 to day 180, for a temperature of heat transfer fluid of 30°C.

From Fig. 10, we can see that after 100 – 110 days, heat accumulates slower.

3. Conclusions

The paper presents an approximative analytical solution used to determine the heat seasonally stored underground. We used different solutions to evaluate the numerical results, in order to develop a model for underground heat storage. This mathematical model can now be used to determine the optimal temperature of the heat transfer fluid and charging time for different types of soil and also to evaluate the volume of soil that is necessary for storing heat undergound. Further researches will be on applications of determining discharge rate of undergound heat.

Nomenclature

R – thermal resistance, [(K·m)/W]
k – thermal conductivity, [W/(K·m)]
q – heat flux, [W/m^2]
T – temperature, [K]
x – distance from heat flux to measured temperature, [m]
h – heat convection coefficient, [W/(m^{2}K)]
t – time, [s]
Q – heat, [J]
A – wall surface, [m^2]
C_v – volumetric heat capacity, [J/(m^3·K)]
C_p – specific heat capacity, [J/(kg·K)]
ρ – density, [g/m^3]

Greek
δ – soil particle dimension, [m]
α – thermal diffusivity, [m^2/s]

Subscripts
s – series
p – parallel
t – thermal
i – index number
a – air
w – water
sm – sand minerals
cm – clay minerals
om – organic matter
f – heat transfer fluid
0 – initial
pw – plane wall
e - end
ac – acumulated

am – arithmetic mean
gm – geometric mean
hm – harmonic mean
lg – logarithmic mean

REFERENCES

Blasch K.W., *Streamflow Timing and Estimation of Infiltration Rates in an Ephemeral Stream Channel Using Variably Saturated Heat and Fluid Transport Methods*, Doctoral Dissertation, Hydrology (2003).

Cengel Y.A., Gajar A.J., *Heat and Mass Transfer*, Fifth Edition (2015).

Diersch H.-J.G., Bauer D., 7 - *Analysis, Modeling and Simulation of Underground Thermal Energy Storage* (*UTES*) *Systems*, In Woodhead Publishing Series in Energy, Edited by Luisa F. Cabeza, Woodhead Publishing, 2015, Pages 149−183, Advances in Thermal Energy Storage Systems, http://dx.doi.org/10.1533/9781782420965.1.149.

Evett S.R., Agam N., Kustas W.P., Colaizzi P.D., Schwartz R.C., *Soil Profile Method for Soil Thermal Diffusivity, Conductivity and Heat Flux: Comparison to Soil Heat Flux Plates*, Advances in Water Resources, 50, 41-54 (2012).

Lo Russo S., Civita M.V., *Open-Loop Groundwater Heat Pumps Development for Large Buildings: A Case Study*, Geothermics, 38, 335-345 (2009).

Lo Russo S., Taddia G., Baccino G., Verda V., *Different Design Scenarios Related to an Open Loop Groundwater Heat Pump in a Large Building: Impact on Subsurface and Primary Energy Consumption*, Energy and Buildings, Vol. 43, Issues 2–3, February–March 2011, pp. 347-357, http://dx.doi.org/10.1016/j.enbuild.2010.09.026 (http://www.sciencedirect.com/science/article/pii/S0378778810003464).

Luo J., Rohn J., Bayer M., Priess A., *Thermal Performance and Economic Evaluation of Double U-Tube Borehole Heat Exchanger with Three Different Borehole Diameters*, Energy and Buildings, Vol. 67, December 2013, pp. 217-224, http://dx.doi.org/10.1016/j.enbuild.2013.08.030 (http://www.sciencedirect.com/science/article/pii/S0378778813005276).

Schibuola L., Tambani C., Zarrella A., Scarpa M., *Ground Source Heat Pump Performance in Case of High Humidity Soil and Yearly Balanced Heat Transfer*, Energy Conversion and Management, 76, 956-970 (2013).

Taylor & Francis, Soil Science - Components and Properties of Soil, 2006.

Yumrutas R., Unsal M., *Energy Analysis and Modeling of a Solar Assisted House Heating System with a Heat Pump and an Underground Energy Storage Tank*, Solar Energy, 86, 983-993(2012).

Zhang H.-F., Ge X.-S., Ye H., Jiao D.-S., *Heat Conduction and Heat Storage Characteristics of Soils*, Applied Thermal Engineering, Vol. 27, Issues 2–3, February 2007, pp. 369-373, http://dx.doi.org/10.1016j.applthermaleng.2006.07.024.

** *Encyclopedia of Soil Science*, Chesworth, Edited by Ward, Dordrecht, Netherland, 2008.

EVALUAREA ENERGIEI TERMICE SOLARE STOCATĂ SUBTERAN

(Rezumat)

Această lucrare prezintă o soluţie analitică aproximativă utilizată pentru a determina căldura stocată sezonier în subteran. Acest model a fost aplicat pentru o perioadă de 180 de zile, având în vedere condiţii de contur de speţa a treia. Solul ca sistem de stocare a energiei, a fost întotdeauna considerat a fi un mediu omogen cu proprietăţi evaluate experimental. Domeniul conductivităţii termice a solului, a fost evaluat aproximativ, în funcţie de conductibilitatea termică a compuşilor solului. S-au presupus două modele în calculul conductivităţii termice aparente a solului, serial şi paralel. Aceste modele folosesc analogia dintre conductivitatea termică şi conductivitatea electrică. Volumul fiecărui compus depinde de concentraţia acestuia în sol. Această soluţie a analitică aproximativă poate fi adaptată la compoziţia reală a solului, potrivit datelor colectate prin studii geologice. Căldura stocată subteran în timpul sezonului ,,cald", din primăvară până în toamnă, a fost calculată ţinând cont de mărimea volumului de pământ subteran de încălzit, funcţia câmpului de temperatură şi conductivitatea termică aparentă.

BULETINUL INSTITUTULUI POLITEHNIC DIN IAŞI
Publicat de
Universitatea Tehnică „Gheorghe Asachi” din Iaşi
Volumul 62 (66), Numărul 1, 2016
Secţia
CONSTRUCŢII DE MAŞINI

EMISSION PERFORMANCE OF DIESEL ENGINE BY FUELLING IT WITH DIESEL-BIODIESEL BLENDS

BY

FAZAL UM MIN ALLAH[*]

University of Craiova, Romania,
Faculty of Mechanics

Received: April 23, 2015
Accepted for publication: June 10, 2015

Abstract. Biodiesel is sustainable fuel obtained from renewable resources. The purpose of this paper is to determine the suitability of diesel-biodiesel blends for Kipor KDE-6500E diesel engine. Emission characteristics are determined with the help of VLT-4588 exhaust gas analyzer. The experiments are performed with D100, B10, B20 and B30 at different loading conditions. CO_2, O_2 and HC emissions are measured to determine the performance of the biodiesel blends. There is considerable decrease in CO_2 and HC emissions by increasing the biodiesel blend ratio.

Keywords: biodiesel; diesel engine; emission analysis.

1. Introduction

Conventional energy resources make the major share of fuel consumption. This results in climate change and environmental hazards (Abas *et al*., 2015). Alternate or renewable energy resources can be used to produce environment friendly fuels. Biodiesel is a substitute to the diesel fuel derived from renewable resources (Elbehri *et al*., 2013). Romania has high potential of

[*]Corresponding author; *e-mail*: fazaluminallah@hotmail.com

producing biodiesel. This is estimated 523toe of theoretical potential to produce biodiesel from edible and non-edible resources (Dusmanescu *et al*., 2014; Patrascoiu *et al*., 2013). Biodiesel can be used directly in diesel engines without further modification. The usage of diesel-biodiesel blends can decrease CO_2 emissions by 78% while NO_x emissions will increase slightly but can be controlled by using fuel additives (US EPA., 2002). Most of the researchers have found the significant decrease in CO_2 emissions and slight increase in NO_x emissions by the direct usage of biodiesel in diesel engines (Shahir *et al*., 2015a, 2015b). In the present work, biodiesel is obtained from sunflower oil. Emission performance of KDE 6500E diesel generator is measured with the help of VLT-4588 gas analyzer.

2. Materials and Methods

2.1. *Experimental Setup*

2.1.1. *Biodiesel Standards*. Biodiesel is obtained from a tranesterification of sunflower oil. The physical and chemical properties of biodiesel lie within the limits of standard EN 14214 given below.

Table 1
EN-14214 (*Rutz and Janssen, 2006*)

Property	EN-14214 Standard
Density at 15°C	860-900 kg/m^3
Kinematic viscosity at 40°C	3.5-5.0 mm^2/sec
Flash Point	> 101°C
Sulphur content	≤ 10 mg/kg
Cetane number	≥ 51
Oxidation stability at 110°C	≥ 6 h
Acid value	≤ 0.5 mgKOH/kg
Iodine value	≤ 120 mgIod/g
Water content	≤ 500 mg/kg
Total contamination	≤ 24 mg/kg

2.1.2. *Diesel Engine and Exhaust Gas Analyzer*. KDE 6500E diesel generator is used to determine the emission performance of biodiesel blends. The specifications for the engine are given in Table 2.

Table 2
Diesel Engine Specifications

Engine Model	KM186FA
Rated frequency	50 Hz
Rated power	4.5 kVA
Maximum Power output	5 kVA
Rated speed	3000 rpm
DC output	12 V/8.3 A
Engine type	Single cylinder vertical four sttroke direct injection
Cylinder capacity	418 ml
Compression ratio	19:1
Cooling system	with air
Rated Voltage	230 V

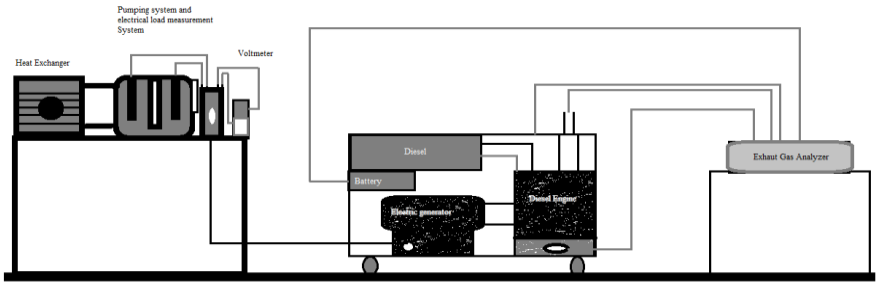

Fig. 1 – Experimental setup scheme.

The experimental setup can be described by a scheme given in Fig. 1. Exhaust gas analyzer is attached after starting the engine. The measurements are recorded by using different blends of biodiesel at different loading condition adjusted by resistances and voltmeter. The electric current is measured at different loads. The power is calculated by the equation given below.

$$P = I \times U \tag{1}$$

where: I is the electric current in Amperes, U is voltage in volts while P is power in Watts.

3. Results and Discussions

Graphical representation of the results obtained from the experiments is given below.

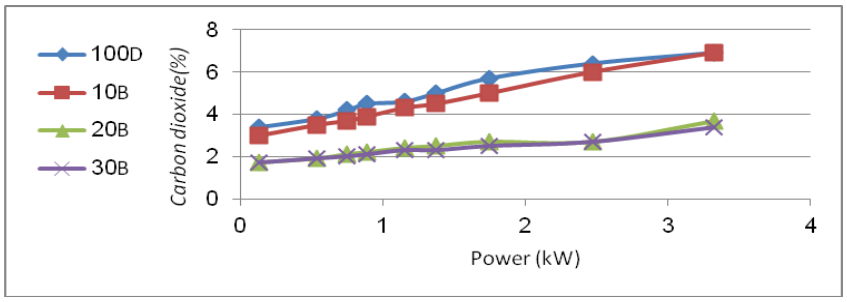

Fig. 2 – CO_2 Emissions for diesel and biodiesel blends.

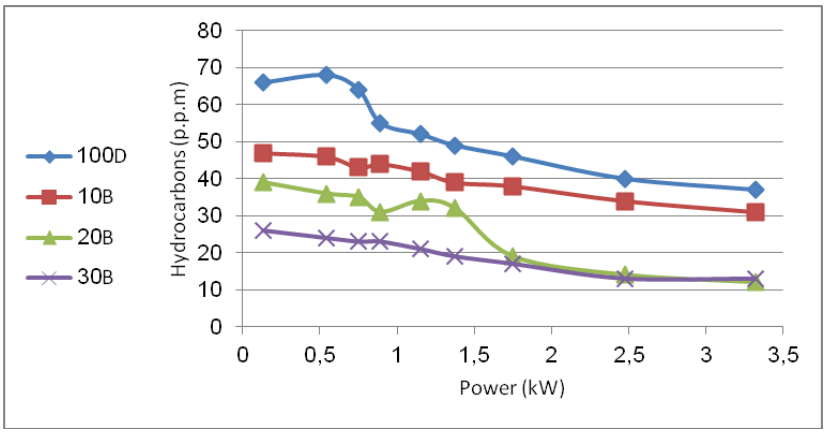

Fig. 3 – CO_2 Emissions for diesel and biodiesel blends.

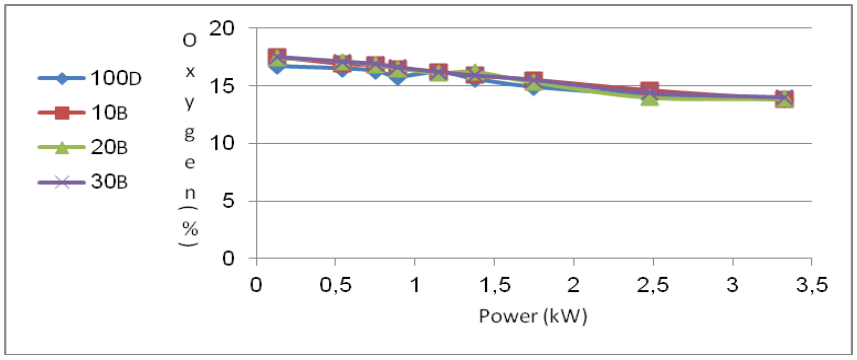

Fig. 4 – O_2 Emissions for diesel and biodiesel blends.

Considerable decrease in CO_2 and HC emissions can be observed by increasing the biodiesel blend. There is no significant change in O_2 emissions. Lower values of HC and CO_2 emissions make it possible for its commercial usage.

4. Conclusions

1. Biodiesel is renewable fuel derived from renewable energy resources and can be directly be used in diesel engines.

2. Diesel-biodiesel blends derived from sunflower exhibit standard physical and chemical properties which make them suitable for diesel engine as fuel.

3. CO_2 and HC emissions can be reduced by increasing blend ratio of biodiesel. An investigation of B10, B20 and B30 shows lowest emissions for B30.

4. There is no significant change in O_2 emissions is observed.

5. Further research is required in bringing these blends in fuel market. Transportation sector of Romania can benefit from this research within European biofuel targets and laws.

Acknowledgements. The author would like to thank the staff of the Thermodynamics Laboratory at the Faculty of Mechanics, Craiova.

REFERENCES

Abas N., Kalair A., Khan N., *Review of Fossil Fuels and Future Energy Technologies,* Futures, **69**, 31−49, 2015.

Dusmanescu D., Andrei J., Subic J., *Scenerio for Implementation of Renewable Energy Sources in Romania,* Procedia Economics and Finance, **8**, 300−305, 2014.

Elbehri A., Segerstedt A., Liu P., *Biofuels and the Sustainability Challenge,* Food and Agriculture Organization of the United Nations, 2013.

Patrascoiu M., Rathbauer Josef, Negrea M., Zeller R., *Perspectives of Safflower Oil as Biodiesel Source for South Eastern Europe* (*Comparative Study: Safflower, Soybean and Rapeseed*), Fuel, **111**, 114−119, 2013.

Rutz D., Janssen R., *Overview and Recommendations on Biofuel Standards for Transport in the EU,* Project: Biofuel Marketplace, WIP Renewable Energies Germany, 2006.

Sahir S.A., Masjuki H.H., Kalam M.A., Imran A., Ashraful A.M., *Performance and Emission Assessment of Diesel-Biodiesel-Ethannol/Bioethanol Blend as a Fuel in Diesel Engines: A Review,* Renewable and Sustainable Energy Reviews, **48**, 62−78, 2015a.

Sahir V.K., Jawahar C.P., Suresh P.R., *Comparative Study of Diesel and Biodiesel on CI Engine with Emphasis to Emissions-A Review,* Renewable and Sustainable Energy Reviews, **45**, 686−697, 2015b.

US Environmental Protection Agency, *A Comprehensive Analysis of Biodiesel Impacts on Exhaust Emissions,* Air and Radiation, 2002.

PERFORMANŢA DE EMISIE A MOTORULUI DIESEL DE ALIMENTARE CU DIESEL-BIODIESEL DE AMESTECURI

(Rezumat)

Biodiesel-ul este un combustibil obţinut din resurse regenerabile. Scopul acestei lucrări este de a determina posibilitatea folosirii amestecurilor biodiesel-motorina pentru alimentarea unui generator alimentat de un motor diesel - Kipor KDE-6500E. Emisiile poluante sunt măsurate cu ajutorul analizorului de gaze tip VLT-4588. Experimentele au fost efectuate în cazul alimentării motorului cu motorină şi amestecuri B 10, B 20 şi B 30 pentru diferite condiţii de încărcare. Au fost măsurate emisiile de CO_2, O_2 şi HC pentru determinarea performanţelor obţinute în urma folosirii amestecurilor biodiesel-motorină. Se poate observa o scădere considerabilă a emisiilor de CO_2 şi HC pe măsura creşterii amestecului biodiesel-motorină.

BULETINUL INSTITUTULUI POLITEHNIC DIN IAŞI
Publicat de
Universitatea Tehnică „Gheorghe Asachi” din Iaşi
Volumul 62 (66), Numărul 1, 2016
Secţia
CONSTRUCŢII DE MAŞINI

THE COMPUTED THERMODYNAMIC PARAMETERS OF SALICYLIC ACID

BY

ANDREEA CELIA BENCHEA, MARIUS GĂINĂ and DANA ORTANSA DOROHOI*

"Alexandru Ioan Cuza" University of Iaşi, Romania,
Department of Physics

Received: April 28, 2015
Accepted for publication: May 28, 2015

Abstract. Some thermodynamic parameters (free energy, entropy, volume, mass) and QSAR properties of molecules (dipole moment, polarizability, refractivity, energy values HOMO and LUMO) were determined using the HyperChem 8.0.6 program. The computed parameters have a significant role in estimation the therapeutic action in the human body. Quantum-mechanical calculations made by us can provide useful information about stability, reactivity and structure of pharmaco-therapeutic compounds.

Keywords: HyperChem 8.0.6; salicylic acid; QSAR properties; thermodynamic parameters.

1. Introduction

Salicylic acid (or 2-hydroxybenzoic acid), has an -OH group adjacent to a carboxyl group. This colorless and crystalline organic acid, is widely used in organic synthesis and functions as a hormone made from plant which generates a major impact on growth and development of plants, photosynthesis, transpiration, ion uptake and transport (Ştefănescu *et al*., 2004).

*Corresponding author; *e-mail*: ddorohoi@uaic.ro

Salicylic acid is the best known chemical compound similar, but not identical, to the active component of aspirin. It is a basic ingredient for multiple products indicated in the treatment of skin diseases (acne, psoriasis, corns, warts, follicular keratosis, dandruff). Salicylic acid salts and esters are known as salicylates. Salicylic acid works as a keratolytic and bacteriostatic agent, opens clogged pores and neutralizes bacteria inside, allowing room for new cell growth (Madan and Levitt, 2014).

Unripe fruits and vegetables are natural sources of salicylic acid, especially blackberries, blueberries, cantaloupes, grapes, figs, kiwi fruits, apricots, green pepper, olives, tomatoes, radish, chicory, mushrooms. Some herbs and spices contain quite high amounts, while meat, poultry, fish, eggs and dairy, legumes, grains, nuts, cereals, only almonds, peanuts, water have significant amounts (Swain *et al*., 1995). Salicylic acid is known for its ability to relieve pain and reduce fever. These medicinal properties have been known since Antiquity and it is used as an anti-inflammatory. In modern medicine, salicylic acid and its derivatives are used as components of some rubefacient products (Tarţău and Mungiu, 2007).

2. Theoretical Background

2.1 Fundamentals of Thermodynamics

Thermodynamics studies the properties of the general macroscopic physical systems and their laws of evolution, taking into account all forms of movement and the heat. The various activities of living organisms means, a suite of conversions of energy, more complex, governed by physical laws of converting one form of energy to another (Lazăr, 2013).

A thermodynamic system is a set of macroscopic size bodies, with specific volume, consisting of molecules and atoms which are in a constinuous movement and disordered by interacting with the external environment as a whole. The system behavior is determined by the internal properties and its interaction with the outside.

From the point of view of the relations with the external environment, systems are of three types: isolated systems (outside of any substance does not change, no energy), closed systems (energy only exterior changes, but not the substance), open systems (exterior changes both substance and energy).

All living organisms are thermodynamically open systems and biological processes are irreversible thermodynamic processes. Steady state of a system is called equilibrium if all the parameters characterizing it does not vary over time and feeds are not caused by external sources that involve transport of the substance. Switching system from initial state to a final state, passing through intermediate states, it is called thermodynamic process or transformation of state (Cristea *et al*., 2006).

Classification of thermodynamic parameters:

a) according to their dependence on the number of particles (N):

− intensive parameters: does not depend on the extent of the system and have the same value in the balance throughout the system (temperature T, pressure p, chemical potential μ);

− extensive parameters: depend on the extent of the system (volume V, mass m, entropy S, the number of particles in the system N). They have the property of being additive.

b) according to their dependence on the position of surrounding bodies:

− external parameters: systems depend on the environment (the intensity of an external field, volume, surface area of a liquid);

− internal parameters: depends on the system considered (pressure, temperature, density, electrical polarization, coefficient of tension of a liquid).

2.2. Molecular Modeling

Molecular modeling is used in many fields such as chemistry, physics, biology, medicine, pharmacy and allows graphical representation of a molecule configuration and calculation of physico-chemical its parameters.

In the pharmacological research, molecular modeling plays an important role. Implemented in various molecular modeling programs, these methods are used to determine properties of drugs found in draft before the actual synthesis.

Molecular modeling methods are numerous, mostly relying on the principles of quantum mechanics and Schrödinger's equation solving (Gottlieb *et al*., 1999) which can be written as:

$$H\,\psi = E\,\psi \tag{1}$$

where: H is the Hamiltonian operator, E and total energy of the system ψ is the wave function of the system (which depends on the coordinates of cores and electrons).

For molecule Schrödinger's equation can be solved only with some approximations. A first approximation was carried out by Born and Oppenheimer. He considers that the motion of cores in a molecule can be separated from that of the electrons, given that the mass of the electron is much smaller than a core.

The most important methods that are used in molecular modeling programs are (Humelnicu, 2003): ab-initio methods, empirical methods, semi-empirical methods. The most important methods semi - empirical: AM1, PM3.

In addition to the methods mentioned above, in recent years there was an expansion of the two methods, the method of molecular dynamics and Monte

Carlo method, which refers to theoretical models that takes an intermediate between theory and experiment, called numerical methods.

Among the most used molecular modeling programs include: Spartan, Gaussian and HyperChem. Most molecular modeling techniques based on the principles of quantum mechanics and Schrödinger's equation solving. Depending on the parameters studied molecular system that are intended to be obtained choosing one or another method.

3. Experimental Part

HyperChem 8.0.6 (www.hyper.com) is a sophisticated molecular modelling program which permits to build and analyze different molecular structures and to determine their physico-chemical properties.

The PM3 method (Parametric Method number 3) from computational chemistry is a semi-empirical method for the quantum calculation of molecular structure. PM3 (Stewart, 1989) uses the Hamiltonian and it is parameterized to reproduce a large number of molecular properties.

In order to generate the spatial chemical structure of each studied molecule, two-dimensional structure of the molecule shall be build step-by-step by drawing. Then hydrogen atoms are automatically added and chemical structure is converted into one 3D.

The first step in getting the main characteristic parameters of molecules is to optimize the molecular structure to obtain a configuration characterized by a minimum free energy. This is usually done using the algorithm Polak - Ribiere with maximum gradient set at 0.001 kcal /(mol*Å).

After optimization is achieved, the theoretical properties of the studied compound are calculated. It aimed to obtaining the value of total energy, the bonding energy, the heat of formation, the energy of frontier orbitals, HOMO (Occupied Molecular Orbital Highest) and LUMO (Lowest Unoccupied Molecular Orbital), the dipole moment, the polarizability and parameters QSAR (Quantitative Structure - Activity Relationship).

4. Results and Discussions

A representation of the molecular structure optimized which contain the values of the reactivity indices is called the reactive molecular diagram. The optimized structure of salicylic acid using the HyperChem 8.0.6. program is represented in Fig. 1.

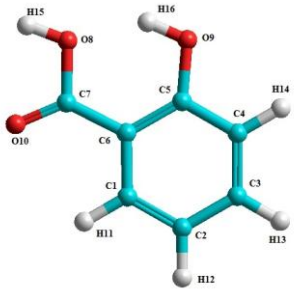

Fig. 1 − The optimized structure of salicylic acid and the denomination of the atoms (colors: red is oxygen, green is carbon, white is hydrogen).

The symmetry (Lide, 2005) is a very powerful tool established on the basis of Hyperchem. Salicylic acid belongs to the CS class symmetry: the molecules of this group are planar and they have only one element of symmetry; the plane of the molecule.

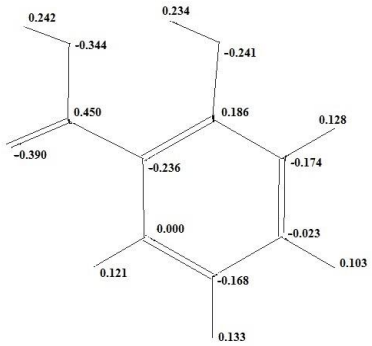

Fig. 2 − The atomic charges computed by HyperChem.

It is seen from Fig. 2 that the negative charges are located near C and O atoms (the highest negative value is -0.390 in O10 atom), and the positive charges are located near H atoms (the highest positive value is 0.450 in C7 atom).

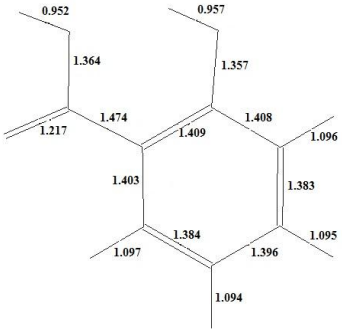

Fig. 3 − The computed bond lengths of molecule (in Å).

The simple bonds C6-C7, C4-C5 are longer than the rest of simple and double bonds than C1-C2, C3-C4 and C7-O10 (Fig. 3). The bond lengths O8-H15 and O9-H16 are the shortest lengths have values below 1 Å.

The energy levels of the molecular orbitals border HOMO (Highest Occupied Molecular Orbital) and LUMO (Lowest Unoccupied Molecular Orbital) for salicylic acid molecule give information on the possible electronic transition. They are highlighted in Fig. 4 (color: green is positive value and blue is negative value).

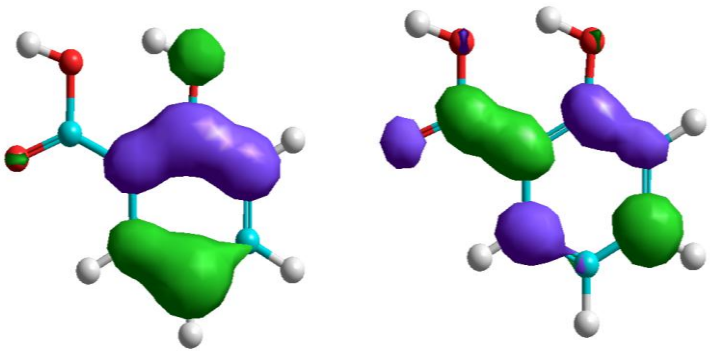

Fig. 4 − The frontier orbitals: a) HOMO and b) LUMO (eV).

The electrophilic attack occurs most likely to the atomic site with a high density of orbital HOMO while nucleophilic attack site is correlated with atomic high-density of orbital LUMO.

The ionization potential (I) and electron affinity (A) can be estimated from the HOMO and LUMO energy values by applying Koopmans theorem (Koopmans, 1934):

$$I = -E_{HOMO} \quad (2)$$

$$A = -E_{LUMO} \quad (3)$$

Table 1

The Values Energies for Salicylic Acid Molecule in the Ground State

Total energy, [kcal/mol]	−41582.53
Heat of formation, [kcal/mol]	−113.079
Binding energy, [kcal/mol]	−1800.599
Electronic energy, [kcal/mol]	−184688.456
Nuclear energy, [kcal/mol]	143105.926
E_{HOMO}, [eV]	−9.456
E_{LUMO}, [eV]	−0.598
$\Delta E = \lvert E_{HOMO} - E_{LUMO} \rvert$, [eV]	8.858

The stability of the studied molecular structure is given by the higher negative values of total energy.

The biological activity of a compound can be estimated on the basis of the energy difference ΔE frontier orbitals. This difference represents the smallest electronic excitation energy which is possible in a molecule.

The surface distribution of molecular electrostatic potential, is an indicator of the specific reactive regions of the molecule.

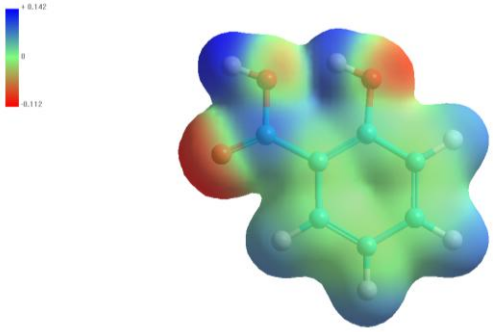

Fig. 5 − 3D geometry of the distribution electrostatic potential.

The three-dimensional geometry of molecular electrostatic potential distribution (Fig. 5), highlights the existence of three regions with increased electronegativity in which oxygen atoms are involved, and that play a role in their coupling to different structures in which ions are positively charged.

Quantitative Structure - Activity Relationships (QSAR) correlate the molecular structure or properties derived from molecular structure with a particular chemical or biochemical activity (Gallegos, 2004). This method is widely used in pharmaceutical chemistry in the environment and in the search for certain properties.

Table 2

QSAR Parameters Calculated by HyperChem

Surface area, [Å^2]	228.00
Volume, [Å^3]	410.17
Mass, [u.a.m]	138.12
Hydration energy, [kcal/mol]	−12.19
Log P	−0.04
Refractivity, [Å^2]	38.56
Dipole moment, [D]	2.17
Polarizability, [Å^3]	13.63

The hydration energy is defined as the energy absorbed when the substance is dissolved in water.

A negative value of log P indicates the hydrophilicity, for the studied compound, that plays an important role in biochemical interactions (Parthasarathi *et al*., 2012).

Hydrophobic drugs tend to be more toxic because, in general, are kept longer, have a wider distribution in the body, are somewhat less selective in their binding to proteins and finally are often extensively metabolized. Therefore ideal distribution coefficient for a drug is usually intermediate (not too hydrophobic nor too hydrophilic).

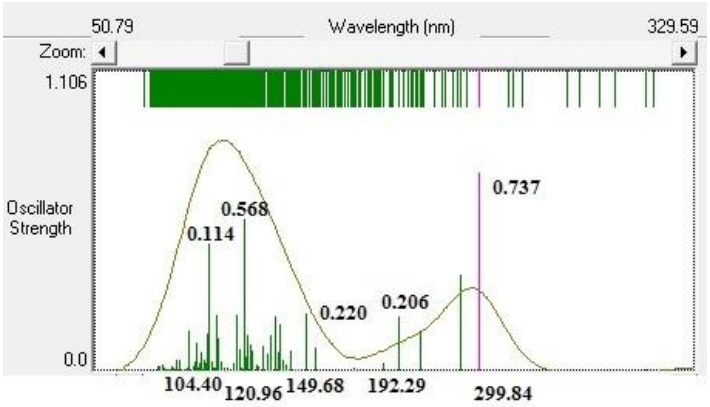

Fig. 8 − The electronic absorbtion spectrum of salicylic acid.

The highest peak corresponding to the absorption bands is at 299.84 nm and it has the oscillator strength with the value of 0.737 (Fig. 8).

The thermodynamic parameters calculated with HyperChem 8.0.6. at too temperatures, do not show big differences (Table 3).

Table 3

Thermodynamic Parameters Determinated Using HyperChem

Temperature	298.15 K	0 K
Entropy, [kcal/mol/deg]	0.08951	0.00509
Free energy, [kcal/mol]	−41528.1	−41582.5
Heat capacity, [kcal/mol/deg]	0.03171	0.00596
Internal energy, [kcal/mol]	−41501.4	−41582.5

In the Kelvin scale the absolute zero temperature (0 K) is the lowest possible and in substance no more energy as heat. The normal room temperature is 298.15 K equivalent to 25°C. In the vicinity of absolute zero (zero Kelvin), the entropy of a thermodynamic system is approximately constant.

The internal energy is a function of the state which represents the total energy of the thermodynamic system that includes the energy for all forms of motion and interaction between the particles of the system (the energy of translational motion, rotation of the molecules, the energy of oscillation of the atoms in the molecules).

From Table 4 shows that the reaction enthalpy (ΔHf and ΔHc) has a negative value such as the reaction enthalpy of a substance is less, the substance is more stable.

Table 4
Condensed Phase Thermochemistry Data -Solid
(http://en.wikipedia.org)

Density, [g/cm^3]	1.443 (20°C)
Pressure, [mPa]	10.93
Acidity, [pKa]	2.97 (25°C)
Melting point, [K]	431.8
Heat capacity, [J/mol*K]	160.9
Entropy, [J/mol*K]	172.4
Enthalpy of formation, [kJ/mol]	−582.45
Enthalpy of combution, [kJ/mol]	−3029.6

The acid dissociation constant pKa, for an acid is a direct consequence of the underlying thermodynamics of the dissociation reaction. A high value of pKa indicates a small degree of disociation at a given pH. The compounds which have pKa value between −2 and 12, are acids. In this case (Table 4) salicylic acid molecule is a weak acid.

5. Conclusions

1. The semi-empirical PM3 method of the program HyperChem 8.0.6. was used to characterize salicylic acid.

2. Were determined the physico-chemical parameters specific to each molecules: the bond lengths, the atomic charges, the formation energy, the binding energy, the molecular descriptors QSAR, the mass, the volume, the dipole moment, the polarizability, the total energy and the energies border).

3. Using molecular modeling programs one can be determined the vibration and electronic spectra of the compound studied. Obtaining by modeling the distribution of molecular electrostatic potential reactive sites led to the identification of the molecules studied.

4. Using some of the program options one could determine some thermodynamic parameters (entropy, enthalpy, free energy).

5. Even if the values obtained by these theoretical methods are slightly different from those experimental they can provide an overview on the compound studied by helping researchers to make "adjustments" required to create a drug as safely and effectively.

Acknowledgments. This work was supported by the strategic grant POSDRU/159/1.5/S/137750, Project "Doctoral and Postdoctoral programs support for increased competitiveness in Exact Sciences research" cofinanced by the European Social Found within the Sectorial Operational Program Human Resources Development 2007 – 2013.

REFERENCES

Cristea M., Popov D., Barvinschi F., Damian I., Luminosu I., Zaharie I., *Fizic*a. *Elemente fundamentale*, Edit. Politehnica, Timişoara, 2006.

Gallegos S.A., *Molecular Quantum Similarities in QSAR: Applications in Computer – Aided Molecular Design*, Ph. D. Thesis, Universitat de Girona, 2004.

Gottlieb I., Dariescu M.A., Dariescu C., *Mecanică cuantică*, Edit. Bit, 1999.

http://en.wikipedia.org/wiki/Salicylic_acid, accessed may 2015.

Humelnicu I., *Elemente de chimie teoretică*, Edit. Tehnopress, Iaşi, 2003.

Koopmans T., *Uber die Zuordnung von Wellenfunktionen und Eigenwerten zu den Einzelnen Elektronen Eines Atoms*, Physica (Elsevier), **1**, *1–6*, 104–113, 1934.

Lazăr I., *Elemente de termodinamică biologică* – curs 2013, http://upmf.ub.ro/Ilazar/Cap5termo.pdf, acccesed may 2015.

Lide R.D., *Handbook of Chemistry and Physics*, Boca Raton, Florida, CRC Press, 2005.

Madan R.K., Levitt J., *A Review of Toxicity from Topical Salicylic Acid Preparations*, J. Am. Acad. Dermatol., **70**, *4*, 788–792, 2014.

Parthasarathi R., Subramanian V., Roy D.R., Chattaraj P.K., *Bioorganic & Medicinal Chemistry*, In Advanced Methods and Applications in Chemoinformatics: Research Progress and New Applications, E.A. Castro, A.K. Haghi (Eds.), 2012.

Stewart J.J.P., *Optimization of Parameters for Semi-Empirical Methods I-Method*, Computational Chemistry, **10**, *2*, 209, 1989.

Swain A.R., Dutton S.P., Truswell A.S., *Salicylates in Foods*, Journal of the American Dietetic Association, **85**, *8*, 1995.

Ştefănescu E., Dorneanu M., Rogut O., Tătărîngă G., *Chimie organică*, Vol. **2**, Edit. Cermi, Iaşi, 2004.

Tarţău L., Mungiu O.C., *Analgezice şi antiinflamatoare nesteroidiene*, Ghid Practic, Iaşi, Edit. Dan, 2007.

www.hyper.com (HyperChem, Molecular Visualisation and Simulation Program Package, Hypercube, Gainsville, Fl, 32601).

PARAMETRII TERMODINAMICI CALCULAŢI AI ACIDULUI SALICILIC

(Rezumat)

Utilizând programul HyperChem 8.0.6. au fost determinati unii parametri termodinamici (energia liberă, entropia, volum, masa) şi unele proprietăţile QSAR ale moleculei (moment de dipol, polarizabilitate, refractivitate, valorile energiilor HOMO şi LUMO). Parametrii obţinuţi au un rol important în estimarea acţiunii terapeutice în organism. Calculele cuanto-mecanice realizate de noi pot aduce informaţii utile despre stabilitatea, reactivitatea sau structura compușilor farmaco-terapeutici.

BULETINUL INSTITUTULUI POLITEHNIC DIN IAŞI
Publicat de
Universitatea Tehnică „Gheorghe Asachi” din Iaşi
Volumul 62 (66), Numărul 1, 2016
Secţia
CONSTRUCŢII DE MAŞINI

INFLUENCE OF WORKING FLUID, EXTERNAL AND INTERNAL PARAMETERS ON THE ORGANIC RANKINE CYCLE PERFORMANCE

BY

MAHDI HATF KADHUM ABOALTABOOQ [1], TUDOR PRISECARU[2,*], HORAŢIU POP[2], VALENTIN APOSTOL[2], VIOREL BĂDESCU[2], MĂLINA PRISECARU[2], GHEORGHE POPESCU[2], POP ELENA[2], CRISTINA CIOBANU[2], CRISTIAN PETCU[3] and ANA-MARIA ALEXANDRU[2]

[1]University Politehnica of Bucharest (on leave from the Foundation of Technical Education, AL-Furat Al-Awsat Technical University, Iraq), Department of Mechanical Engineering
[2]University Politehnica of Bucharest, Romania, Department of Mechanical Engineering
[3]Rokura Company

Received: May 10, 2015
Accepted for publication: September 25, 2015

Abstract. In this paper the effect of external and internal parameters on the Organic Rankine Cycle (ORC) performance depending on the working fluid is investigated. The pump efficiency , expander efficiency and ambient temperature are the parameters used. The working fluids considered in the present study are Toluene, n-pentane, R600, HFE7100, HFE7000, R11, R141b, R123, R113 and R245fa. In this study the heat source is waste heat applied from diesel engine. The results show that increasing of ambient temperature has bad effect on thermal efficiency and power of ORC system. As well as with increasing the pump and expander efficiency the thermal efficiency and the power of ORC is increased. The largest exergy loss occurs in evaporator, followed by the condenser, expander and pump, so the focus must be on the evaporator section more than the remaining parts. The exergy rate or irreversibility for pump,

[*]Corresponding author; *e-mail*: tpris@caz.mecen.pub.ro

expander and condenser increase slightly with inlet turbine temperature while the increase in exergy rate for evaporator is higher. The results were compared with result by other authors and the agreement was good.

Keywords: Waste heat recovery–Organic Rankine cycle–Performance.

1. Introduction

One of the methods to improve the thermal efficiency of an internal combustion engine is the usage of, Organic Rankine cycles (ORCs) to recover the waste heat. The available heat which is called as waste heat is transferred to the organic working fluid by an evaporator in an ORC, where the organic working fluid changes from a liquid state to a vapour state under a high pressure. Then, the organic working fluid, which has a high enthalpy, is expanded in an expander, and power is generated. Therefore, the evaporator is an important part of the ORC for an engine waste-heat recovery system. Many studies analysing the ORC performances have been conducted recently (Gewald *et al.*, 2012; Kang, 2012; Vélez *et al.*, 2012). Therefore in this study the effects of external and internal parameters on the (ORC) performance are studied. The internal parameters such as pump efficiency and turbine efficiency while ambient temperature is considered as external parameter. The working fluids considered in the present study are Toluene, n-pentane, R600, HFE7100, HFE7000, R11, R141b, R123, R113 and R245fa (He *et al.*, 2012).

2. Mathematical Model

The working fluid leaves the condenser as saturated liquid and then it is pumped from point (1) to point (2) in isentropic process theoretically while to the point (2r) actually as shown in Fig. 1 (Sun and Li, 2011; Wang *et al.*, 2011; Rentizelas *et al.*, 2009). The pump power can be expressed as (Mago *et al.*, 2007):

$$\dot{W}_{P,\,actual} = \frac{\dot{W}_{P,\,ideal}}{\eta_P} = \frac{\dot{m}_{ref}\left(h_1 - h_{2s}\right)}{\eta_P} = \dot{m}_{ref}\left(h_1 - h_{2r}\right) \tag{1}$$

where: $W_{p,ideal}$ is the ideal power of the pump, $\dot{m}_{ref}$ − the working fluid mass flow rate, η_p − the isentropic efficiency of the pump, h_1 − enthalpy of the working fluid at the inlet and h_{2s} and h_{2r} − the isentropic and actual enthalpies of the working fluid at the outlet of the pump, respectively.

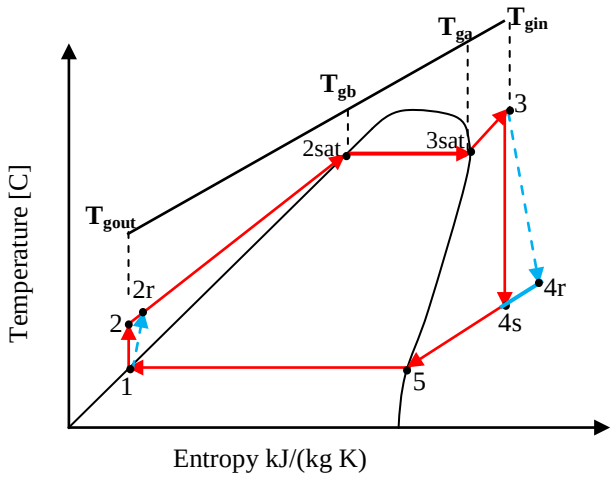

Fig. 1 – T-s diagram for ORC.

The irreversibility rate for uniform flow conditions can be expressed as (Mago *et al*., 2007):

$$\dot{I} = \dot{m}_{ref} T_o \left[\sum_{outlet} s - \sum_{inlet} s + \frac{ds_{system}}{dt} + \sum_k \frac{q_k}{T_k} \right] \tag{2}$$

where: T_k − temperature of each heat source, q_k − heat transferred from each heat source to the working fluid and T_0 − the ambient temperature. In Eq. (2), the contributions of internal or external irreversibilities occurring inside the system or components of the system, a control mass for the system or control volume for each component is taken into account in totality.

Since the system is steady state that is mean $ds_{system}/dt=0$ then the Eq. (2) reduced to:

$$\dot{I} = \dot{m}_{ref} T_o \left[\sum_{outlet} s - \sum_{inlet} s + \sum_k \frac{q_k}{T_k} \right] \tag{3}$$

Assuming only one inlet and one outlet for a single component, for steady-state steady flow processes the Eq. (3) reduces to:

$$\dot{I} = \dot{m}_{ref} T_o \left[(s_{out} - s_{in}) + \frac{q_k}{T_k} \right] \tag{4}$$

For the pump component the heat transferred to the working fluid (q_k) = 0 substitute in Eq. (4) then the final equation of the exergy destruction rate in the pump (irreversibility rate) is:

$$\dot{I}_p = \dot{m}_{ref} T_o \left[(s_{2r} - s_1) \right] \tag{5}$$

where: s_1 and s_{2r} are the specific entropies of the working fluid at the inlet and exit of the pump for the actual conditions, respectively.

The absorbed energy at the evaporator is converted to useful mechanical work by an expander or a turbine. The turbine power is given by Eq. (6):

$$\dot{W}_t = \dot{W}_{t,ideal}\ \eta_t\ = \dot{m}_{ref}\ (h_3\text{-}h_4)\ \eta_t = \ \dot{m}_{ref}\ (h_3\text{-}h_{4r}) \tag{6}$$

where: $W_{t,ideal}$ is the ideal power of the turbine, η_t − the turbine isentropic efficiency, and h_3 and h_{4r} − the actual enthalpies of the working fluid at the inlet and outlet of the turbine. To calculate the exergy destruction rate in the turbine can be expressed as Eq. (7):

$$\dot{I}_t = \dot{m}_{ref} T_o \left[(s_{4r} - s_3) \right] \tag{7}$$

where: s_3 and s_{4r} are the specific entropies of the working fluid at the inlet and exit of the turbine for the actual conditions, respectively. To determine the exergy destruction rate in the evaporator as shown in Eq. (8):

$$\dot{I}_e = \dot{m}_{ref} T_o \left[(s_3 - s_{2r}) \text{-} \frac{(h_3 - h_{2r})}{T_H} \right] \tag{8}$$

Then, the exergy destruction rate in the condenser is calculated from Eq. (9):

$$\dot{I}_c = \dot{m}_{ref} T_o \left[(s_1 - s_{4r}) \text{-} \frac{(h_1 - h_{4r})}{T_L} \right] \tag{9}$$

3. Results

Based on the mathematical model presented above a program has been developed in Engineering Equation Solver (F-chart software) for different refrigerants. The aim is to show the influence of ambient temperature, pump and expander efficiency on the performance of the ORC (thermal efficiency and power output) for same heat input. The working fluids considered in the present study are Toluene, n-pentane, R600, HFE7100, HFE7000, R11, R141b, R123, R113 and R245fa .The choosing of these fluids depending on the type of fluid is dry or isentropic. Six working fluid is dry (R113, R600, HFE7100, HFE7000, n-pentane and Toluene) and four working fluid is isentropic (R245fa, R123, R11 and R141b) and leave it the wet fluid because the disadvantages of this type.

3.1. Effect of Ambient Temperature

Effect of ambient temperature on turbine power and thermal efficiency is shown in Figs. 2 and 3 respectively. It can be observed for all fluids that the turbine power and thermal efficiency decrease with the ambient temperature and from this point the increasing in ambient temperature shows a bad effect on the ORC performance. One can notice that the highest power output is obtained for Toluene while the lowest one for HFE7100. The highest efficiency of the ORC is obtained for toluene and R11 while the lowest is obtained for HFE7100.

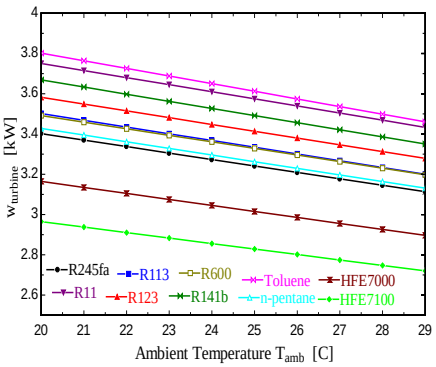

Fig. 2 – Effect of T_{amb} on the Turbine power at Δt_{sup} = 10°C, t_{ev} = 120°C.

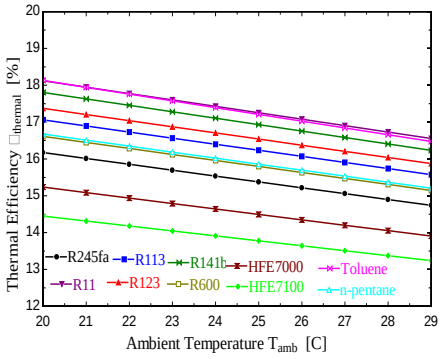

Fig. 3 – Effect of T_{amb} on the thermal efficiency at Δt_{sup} = 10°C, t_{ev} = 120°C.

3.2. Effect of Expander Efficiency and Pump Efficiency

Figs. 4 and 5 show the effect of pump efficiency and expander efficiency on the thermal efficiency and net power at the same time for R245fa. It can be observed from these figures that thermal efficiency and net power increases with the increase in pump and expander efficiency.

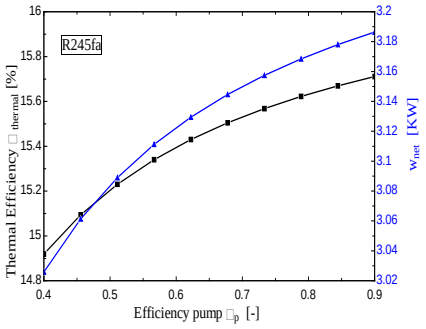

Fig. 4 − Effect of pump efficiency on the thermal efficiency and net power at t_c = 27°C t_{ev} = 120°C.

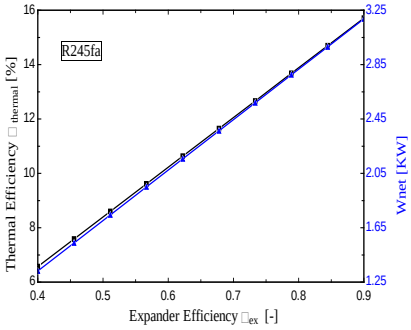

Fig. 5 − Effect of turbine efficiency on the thermal efficiency and net power at t_c = 27°C t_{ev} = 120°C.

From Fig. 6 can be seen the effect of inlet turbine temperature on the irreversibility of components for R245fa as example and from the figure can be seen clearly the largest exergy loss occurs in evaporator, followed by the condenser, expander and pump, therefore it is better to focus on the evaporator section more than the remaining parts. The exergy rate for pump, expander and condenser are increasing slightly while the increase in exergy rate for evaporator is higher. Fig. 7 shows the exergy components for different working fluids.

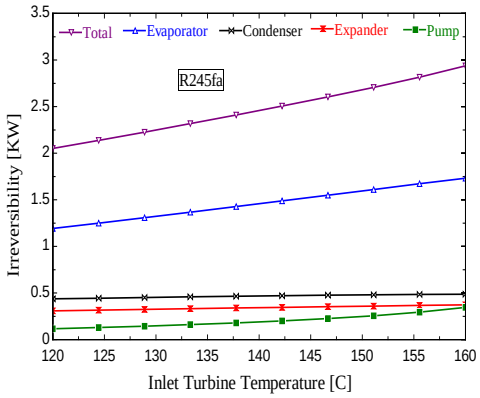

Fig. 6 − Effect of ITT on the components Irreversibility for R245fa.

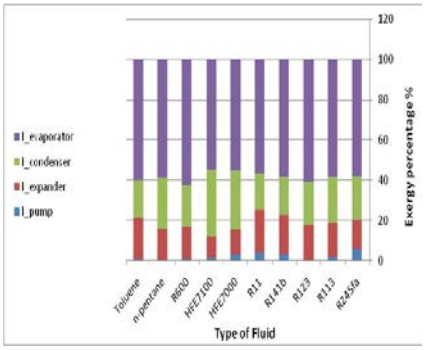

Fig. 7 − Destributed exergy of components Irreversibility for different fluids.

3.3. Comparison Between Present Work and Other Author

To check the validity of the results, it was necessary to compare the results with literature review. The present model and calculation procedure were successfully validated by comparing their results with corresponding results from the literature especially with author (Zhang, 2013) and the comparison were shown in Figs. 8 *a-d*. It can be observed from this figure that paper results are reliable and the agreement is very good.

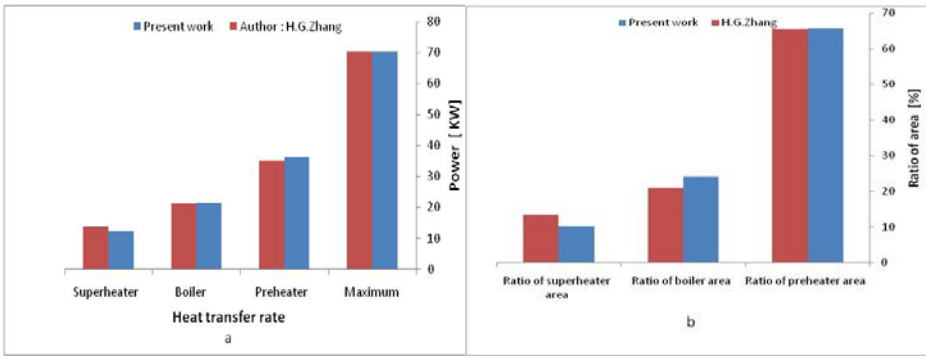

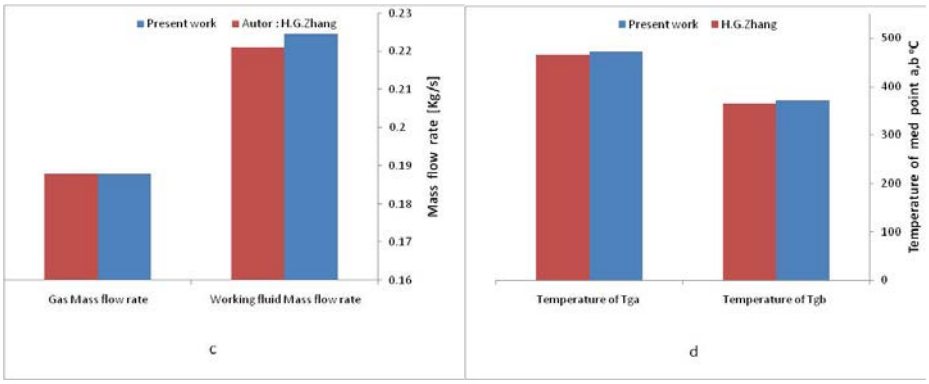

Fig. 8 − Comparison between present work and author: Zhang, 2013.

4. Conclusions

1. The irreversibility of evaporator was the high value while the irreversibility of pump was the smallest and due to that must be focus on the evaporator section more than the remaining parts.

2. It can be observed for all fluids that the turbine power and thermal efficiency decrease with the ambient temperature as example approximately the losses in turbine power is 0.289 KW and 1.43% in thermal efficiency for R245fa because of 9°C increasing in ambient temperature and this is bad effect.

3. From the working fluids under study the Toluene is the best performance and the HFE7100 is the bad performance.

Acknowledgements. One of the authors (M.H.K. Aboaltabooq) acknowledges support from the Ministry of higher education and scientific research of Iraq through grant and the Romanian government through Research grant, "Hybrid micro-cogeneration group of high efficiency equipped with an electronically assisted ORC", 1st Phase Report, 2nd National Plan, Grant Code: PN-II-PT-PCCA-2011-3.2-0059, Grant No.: 75/2012.

REFERENCES

F-Chart Software http://www.fChart.com

Gewald D., Karellas S, Schuster A, Spliethoff H. *Integrated System Approach for Increase of Engine Combined Cycle Efficiency*, Energy Convers Manage, **60**, 36-44 (2012).

He C., Liu C., Gao H., Xie H., Li Y., Wu S. *et al*., *The Optimal Evaporation Temperature and Working Fluids for Subcritical Organic Rankine Cycle*. Energy, **38**, 136-143 (2012).

Kang S.H., *Design and Experimental Study of ORC* (*Organic Rankine Cycle*) *and Radial Turbine Using R245fa Working Fluid*, Energy, **41**, 514-524 (2012).

Mago P.J., Chamra L.M., Somayaji C., *Performance Analysis of Different Working Fluids for Use in Organic Rankine Cycles*, Proc. IMechE, **221**, *3*, 255-263, Part. A: J. Power and Energy (2007).

Rentizelas A., Karellas S., Kakaras E., Tatsiopoulos I., *Comparative Technoeconomic Analysis of ORC and Gasification for Bioenergy Applications*, Energy Convers Manage, **50**, 674-681 (2009).

Sun J., Li W., *Operation Optimization of an Organic Rankine Cycle* (*ORC*) *Heat Recovery Power Plant*, Applied Thermal Engineering, **31**, 2032-2041 (2011).

Vélez F., Chejne F., Antolin G., Quijano A., *Theoretical Analysis of a Transcritical Power Cycle for Power Generation from Waste Energy at Low Temperature Heat Source*, Energy Convers Manage, **60**, 188-195 (2012).

Wang E.H., Zhang H.G., Fan B.Y., Ouyang M.G., Zhao Y., Mu Q.H., *Study of Working Fluid Selection of Organic Rankine Cycle (ORC) for Engine Waste Heat Recovery*, Energy, **36**, 3406-3418 (2011).

Zhang H.G., Wang E.H., Fan B.Y., *Heat Transfer Analysis of a Finned-Tube Evaporator for Engine Exhaust Heat Recovery*, Energy Conversion and Management, **65**, 438-447 (2013).

INFLUENȚA AGENTULUI DE LUCRU ŞI A PARAMETRILOR EXTERNI ŞI INTERNI ASUPRA PERFORMANȚEI CICLULUI ORGANIC RANKINE

(Rezumat)

Lucrarea prezintă un studiu termodinamic privind influenţa parametrilor externi (temperatura ambiantă) şi interni (eficienţa izentropică a pompei şi a detentorului) aupra performanţei ciclului organic Rankine (COR) în funcţie de natura şi tipul agentului de lucru. Ciclurile organice Rankine utilizează ca agent termodinamic substanţe de tipul agenţilor frigorifici şi reprezintă o soluţie tehnică avantajoasă pentru recuperarea căldurii reziduale şi creşterea eficienţei energetice a sistemelor termice. Agenţii de lucru consideraţi în această lucrare sunt toluen, n-pentan, R600, HFE7100, HFE7000, R11, R141b, R123, R113 şi R245fa. Sursa de caldură considerată este căldura reziduala provenită de la gazele de ardere ale unui motor cu ardere internă cu aprindere prin comprimare. Studiul termodinamic s-a realizat pe baza unui program elaborat în Engineering Equation Solver (EES). Rezultatele obţinute arată că puterea furnizată şi eficienţa termică a COR scad cu creşterea temperaturii ambiante şi cresc cu creşterea eficienţei pompei şi a detentorului. Un rezultat important al acestei lucrări arată că pierderea de exergie la nivelul vaporizatorului este cea mai mare fiind urmată de cea la nivelul condensatorului, detentorului şi pompei. Acest rezultat arată că în analiza sistemelor COR o atenţie deosebită trebuie acordată vaporizatorului. De asemenea, pierderile de exergie la nivelul pompei, condensatorului şi detentorului cresc mai puţin pronunţat cu creşterea temperaturii agentului frigorific la intrare în detentor decât la nivelul vaporizatorului. Rezultatele obţinute sunt în concordanţă cu alte date disponibile în literatură pentru aplicaţii similare.

BULETINUL INSTITUTULUI POLITEHNIC DIN IAŞI
Publicat de
Universitatea Tehnică „Gheorghe Asachi” din Iaşi
Volumul 62 (66), Numărul 1, 2016
Secţia
CONSTRUCŢII DE MAŞINI

MODERN SOLUTIONS TO EXPLOIT THE ENERGY POTENTIAL OF COMBUSTIBLE GASES CONTAINED IN GEOTHERMAL WATERS, WITH LOW POWER COGENERATION PLANTS

BY

SORIN DIMITRIU[1,*], ANA MARIA BIANCHI[2] and FLORIN BĂLTĂREŢU[2]

[1]University POLITEHNICA, Bucharest, Romania
Department of Engineering Thermodynamics, Internal Combustion Engines, Thermal and Refrigerating Equipments
[2]Technical University of Civil Engineering, Bucharest, Romania
Department of Engineering Thermodynamics and Thermal Equipment

Received: April 15, 2015
Accepted for publication: June 1, 2015

Abstract. The paper focuses on thermal potential utilization of the geothermal resources from the Olt Valley (Romania, Călimănești, Căciulata area). The three existing drills ensure low enthalpy geothermal water (92–95°C) having, at the exit of the wells, a high content of combustible gases. At present, the gases from the geothermal water, having a rich content of methane (88%), are released into the atmosphere. The paper proposes a few solutions concerning complete exploitation of the energy potential of this geothermal water, using the modern technology of low power cogeneration. We highlight that it is possible to extend the exploitation of the geothermal energy by a viable solution, via which the investment can be recovered in a short time. This work provides solutions in total accordance with the European Directives regarding the increase in energy efficiency, the use of the renewable resources and the environment protection. It was performed a comparative study regarding the efficiency and the costs on energy unit produced, assuming the implementation of these solutions in the central heating system of Călimănești Town.

Keywords: geothermal energy; small power cogeneration.

[*]Corresponding author; *e-mail*: dimitriu47@yahoo.com

1. Introduction

Geothermal energy has been used for centuries, for spa treatments, preparing domestic hot water and heating. It reduces greenhouse gas emission, using an inexhaustible and continuously available source. The European energy policy in this field has never been more important. Renewable energy plays a crucial role in reducing greenhouse gas emissions and other forms of pollution, diversifying and improving the security of energy supply. It is for this reason that the leaders of the European Union have agreed on legally binding national targets for increasing the share of renewable energy, so as to achieve a 20% share for the entire Union by 2020 (EU Commission - Directorate General for Energy, 2011). The problem of the integration of the renewable energy sources and micro cogeneration into a heating or a district heating system is of great interest worldwide. Examples of such applications concern hybrid micro-cogeneration systems (an internal combustion engine integrated with a high efficiency furnace) designed to satisfy both the thermal and power needs of a building (Entchev *et al*., 2013), or renewable energy systems using low enthalpy geothermal energy for district heating (Østergaard and Lund, 2011).

In Romania, the geological research carried out between 1960 and 1980 has proved the existence of significant geothermal resources, mainly in the western part of the country, with an annual geothermal usable potential of about 7,000 TJ (Roşca and Antics, 1999). The Table 1 presents the main characteristics of the most important geothermal deposits from Romania (Roşca *et al*., 2010).

Table 1

The Main Parameters of the Most Important Romanian Geothermal Systems

Parameter	um	Oradea	Borş	Beiuş	Western Plain	Olt Valley	North Bucharest
Reservoir type		carbonate	carbonate	carbonate	sandstone	gritstone	carbonate
Area	km^2	75	12	47	2500	10	350
Depth	km	2.2...3.2	2.4...2.8	2.4...2.8	0.8…2.4	2.7...3.2	2.0...3.2
Drilled wells	tot	14	6	2	88	4	17
Well head tmp.	°C	70…105	120	84	50...90	70...95	51...84
Temp. gradient	°C/km	35...43	45...50	33	37...42	30...35	23...26
Mineralisation	g/l	0.8...1.4	12...14	0.46	2...6	15.7	2.2
Gases	m^3_N/m^3	0.05	5...6.5	–	0.6...2.1	1...2	0.1
Prod. type		Artesian	Artesian	Pumping	Art+Pump	Artesian	Pumping
Flow rate	l/s	4…20	10...15	13...44	4...12	8.5...22	22...28
Oper. wells		11	2	1	18	3	1
Inst. power	MW	58	25	10	30	12.5	35
Main uses:							
space heating	dwellings	2000	–	10500	350	2250	–
sanit. hot water	dwellings	6000	–	10500	1750	2250	–
greenhouses	ha	–	–	–	10	–	–
industrial uses	operation	–	–	–	1	–	–
health bathing	operation	2	–	–	4	6	1

The main uses of geothermal waters are for district heating and the heating of individual buildings, balneology, recreation, greenhouses heating, fishing culture and industrial uses as drying cereals, wood, etc., (ICEMENERG, 2006; Marasescu and Mateiu, 2013). In accordance with EU principles and directives, the Romanian Government approved the "Strategy for the development of renewable energy sources" (HG 1535, 2003). This government decision provides significant increases in research activities and investments to capitalize the geothermal potential with direct economic applications. It has spurred concerns for efficient exploitation and utilization of the geothermal resources but the completion of the projects took a long time and great efforts, due to financial difficulties and problems with the existing laws. Practical projects of the last 10 years are rather modest, being located in some localities of the western part of the country and on the Olt Valley, Vâlcea County. These projects were intended either for modernising the equipment and management of the existing geothermal systems or for the exploitation of new geothermal reservoirs. Some of these projects have involved consultants from Western European countries and received financial support from the European Union (Antal and Roşca, 2008). Given these concerns, the objective of the present paper is to propose a modern solution for the utilization of the energy potential of the geothermal resources, from the area around Călimăneşti Town, Vâlcea County. In this area, the geothermal water is provided by three drillings located on the right-hand side of the Olt River. The three existing drillings provide low enthalpy geothermal water, having the well exit temperature of about 95°C, and a high content of combustible gases, especially methane. A project, developed in 2001–2002, aimed at integrating all geothermal resources from this perimeter into the heating system of Călimăneşti Town (Burchiu *et al.*, 2006). Currently, only one of the wells provides the district heating system with geothermal water. In order to use the entire thermal potential of the geothermal water, the article proposes the recovery of the combustion heat of the gases with modern technology of low power cogeneration units.

2. The Energy Potential of the Gases from Geothermal Water

The Table 2 presents the composition and the amount of gases contained in geothermal water, according to analyses reported at the commissioning of boreholes (Burchiu *et al.*, 2006). The maximum available volume flow for the ensemble of the three drillings is about 50.4 l/s, which is equivalent to an effective thermal potential of 13.2 MW, if the geothermal water after its utilization reaches a temperature of 30°C. It can highlight, at all the three wells, a large amount of gases associated with the geothermal water, having a great content of methane (over 88%) and a low heating value (LHV) of about 32 MJ/m^3_N. The Table 3 presents the energy potential likely to be recovered by burning the combustible gases from the whole flow of the hot

water, actually produced by the all the three existing wells. The available thermal power, at the whole capacity of the wells, is about 3.6 MW.

Table 2
Composition and Ratio of Gases from Geothermal Water

Geothermal water well	#1005 Căciulata	#1008 Cozia	#1009 Călimănești
The water well working parameters during the sample gathering.	Volume flow 32.4 m^3/h Temperature 87°C	Volume flow 57.6 m^3/h Temperature 89°C	Volume flow 28.8 m^3/h Temperature 85°C
The ratio of gases associated with geothermal water (m^3_N/m^3 water)			
Nitrogen (N_2)	0.2638	0.2928	0.3254
Carbon dioxide (CO_2)	0.0247	0.0198	0.0264
Methane (CH_4)	2.1561	1.6545	2.2389
Ethane (C_2H_6)	0.0200	0.0129	0.0193
Propane (C_3H_8)	0.0042	0.0032	0.0028
i-Butane (C_4H_{10})	0.0002	0.0008	0.0003
n-Butane (C_4H_{10})	0.0007	0.0010	0.0003
·*Total*: ·*Combustible gases*	2.4697 2.18 (88%)	1.9850 1.67 (84%)	2.6404 2.26 (86%)
·*LHV* (MJ/m^3_N)	31.7	30.5	30.6

Table 3
The Raw Energetic Potential Possible to be Recovered from Gases Associated with Geothermal Water

Geothermal water well	Water volume flow l/s	Gas ratio m^3_N/m^3 water	Gas temp. °C	Low Heating Value MJ/m^3_N	Thermal power	
					MW	toe/h
Căciulata	9.4	2.470	96	32.0	0.743	0.064
Cozia	23.0	1.985	92	30.5	1.392	0.120
Călimănești	18.0	2.645	92	31.0	1.476	0.127
TOTAL	50.4	2.311*	92.7*	30.9*	3.611	0.311

*mean value

3. The Present Utilization of the Geothermal Resources

The drilling located in the neighbourhood of Căciulata and Cozia are used for local needs. The geothermal water provides a group of hotels and health bathing units, for heating and domestic hot water supply. The high thermal potential of the geothermal water leads to its direct exploitation. The

geothermal water is cooled in heat exchangers, in a cascade manner, in order to use the entirely thermal potential, the basic scheme of the geothermal water distribution being presented in Fig. 1.

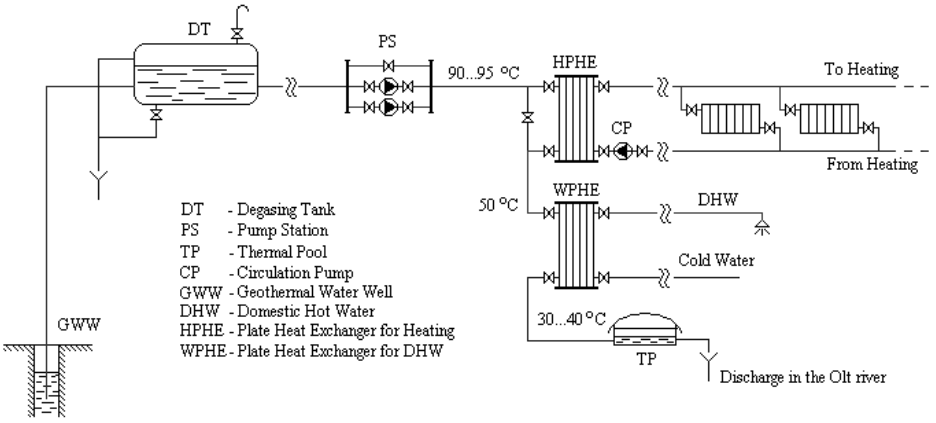

Fig. 1 − The basic scheme of geothermal water utilization.

In the cold season, the geothermal water (having a temperature of 92…95^{o}C) is cooled in a plate heat exchanger, producing the thermal fluid for the heating system. A second heat exchanger produces domestic hot water. The geothermal water, cooled in the two heat exchangers, feeds the thermal pool, after that being discharged in the Olt River at a temperature of about 30°C. In the warm season, the mass flow extracted is reduced, only the heat exchanger for domestic hot water and thermal pool being in use The third drilling is situated at a distance of 1,2 km from Călimăneşti, providing a volume flow of 18 l/s at the same temperature values 92…95°C (Table 3). This locality, beside the tourists which are staying in hotels, has about 8500 permanent habitants; 20% of the habitants are living in apartments connected to a centralized system for thermal energy supply. In the cold season of 2012-2013, 546 apartments were branched to central heating system (ANRSC, 2014). This system has to ensure a thermal need of about 3500 kW for heating and about 500 kW for domestic hot water supply (taking into account the conventional climatic parameters); it was initially designed with three thermal units, equipped with hot water boilers using light liquid fuel. The geothermal water from the nearby well was initially used only for the thermal energy supply of the health bathing units and for the thermal pools. The project of geothermal energy supply was started in 2002 year with internal financing, and was later supported by European funds. Initially, the project included the three wells to provide the centralized heating of Călimăneşti town. Later it was utilized only the available water from the well #1009, situated in vicinity of town. The available volume flow is of 18 l/s, from which about 8 l/s is utilized by a health bathing centre and a hotel; the rest of volume flow (about 10 l/s) being used in the central

heating system of Călimăneşti. In order to include the geothermal water into the heating system, a geothermal heating station was built just near the geothermal well; the geothermal water produces, by using plate heat exchangers, the primary thermal fluid for the heating system, having a temperature of about 85°C. This primary thermal fluid serves to partially cover the heating demand and to completely cover the sanitary hot water preparation.

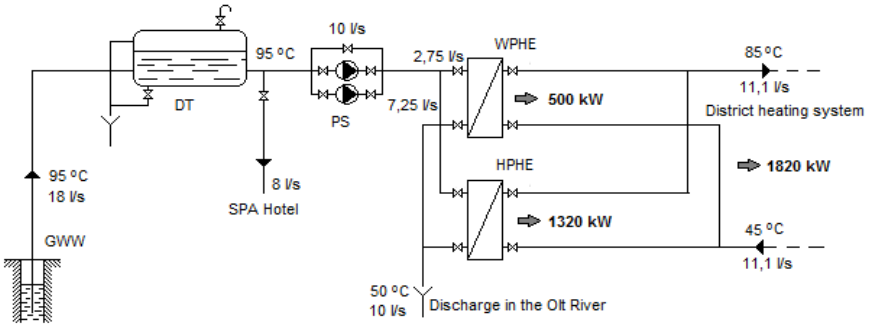

Fig. 2 − The operating scheme of the current geothermal station: GWW – geothermal water well; DT – degassing tank; PS – pumping station; WPHE – plate heat exchanger for domestic hot water; HPHE – plate heat exchanger for heating.

The geothermal heating station with its scheme presented in the Fig. 2, uses a continuous functioning heat exchanger, that completely covers the thermal needs for the sanitary hot water preparation, and another heat exchanger that works only in the cold season, when the heating system is on. Because the temperature of the thermal fluid returned from the both domestic hot water preparation system and heating system is about 45°C, the geothermal water cannot be cooled below 50°C, being discharged in the Olt River at this temperature. In this way, the thermal potential of the geothermal water is not entirely used. Even in these conditions, the use of the geothermal water leads to the complete elimination of the liquid fuel for domestic hot water preparation and to the supply of about 1/3 of the thermal energy needs for heating in the locality of Călimăneşti. In order to cover the peaks and the rest of the thermal energy needs, the oil-fired hot water boilers were maintained. The three district heating plants with oil-fired boilers were transformed in thermal distribution points. The cost of thermal energy produced from geothermal water, is about 0.03 €/kWh, versus 0.1 €/kWh, if the energy is produced in the old oil-fired plants only (ANRSC, 2014).

The primary energy ratio (*PER*) of this combined thermal energy supply system (geothermal and classic) can be determined with the expression:

$$PER = \frac{\dot{Q}}{\dot{Q}_H^{HWB}} \cdot \eta_{HWB} \tag{1}$$

where $\dot{Q}$, [kW] is the total estimated thermal power for the heating system (domestic hot water production and heating), $\dot{Q}_H^{HWB}$, [kW] represents the thermal power needs for heating provided only by the oil-fired hot water boilers and η_{HWB} is the efficiency of the hot water boilers, usualy in range of 0.88...0.92 (Bianchi *et al.*, 2011). Considering $\dot{Q}$ = 4000 kW and $\dot{Q}_H^{HWB}$ = 2180 kW, the obtained value is *PER* = 1.65, which means an improvement of the system efficiency about 83% compared to the previous situation, when the total thermal energy for the heating system was produced only using liquid fuel, in this case the efficiency being $PER = \eta_{HWB} \approx 0.9$.

4. The Recovery of the Combustion Potential of the Gases Using Low Power Cogeneration Units

The simplest solution to utilise this potential consists in the combustion of the gases directly, in the actual oil-fired hot water boilers, completely replacing the liquid fuel. Considering the hot water boilers efficiency of about 90%, the value of the utilisable thermal potential is of about 3.2 MW, the existing heating system having the possibility to work without liquid fuel, taking into account only the burning of combustible gases. However, the best solution is to use the combustible gases to put into action low power cogeneration units such as: gas internal combustion engine units, micro gas turbine units or fuel cell units. The Fig. 3 is presents the schematic diagram of the geothermal station, working together with such a cogeneration unit.

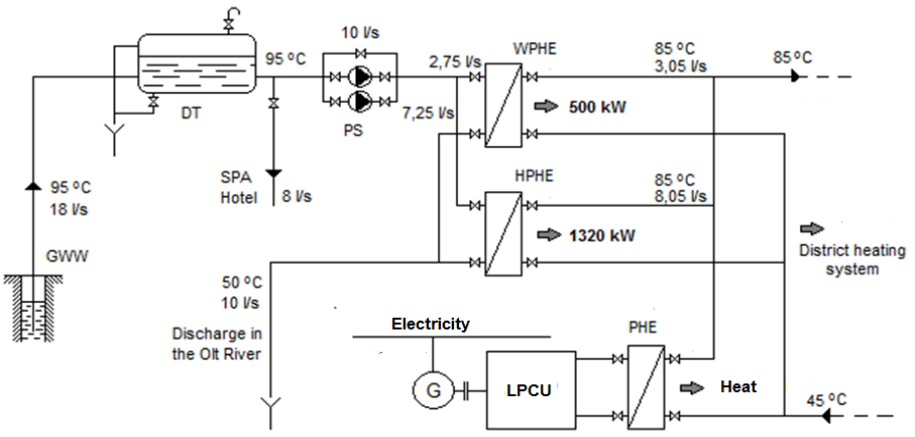

Fig. 3 − The schematic diagram of using a low power cogeneration unit: GWW – geothermal water well; DT – degassing tank; PS – pumping station; WPHE – plate heat exchanger for domestic hot water; HPHE – plate heat exchanger for heating; PHE – plate heat exchanger; LPCU – low power cogeneration unit.

The low power cogeneration unit operates in parallel with the geothermal station, increasing the mass flow of the agent sent into the district heating system. The gas flow obtained from geothermal water allows to put into action the cogeneration unit, an additional amount of heat being delivered into heating system. The electricity obtained in excees can be injected into local public grid.

4.1. The Recovery of the Combustion Potential of the Gases Using Micro Gas Turbine Cogeneration Units

The small gas turbine cogeneration units, using gaseous or liquid fuel, have become commercial and operational around the year 2000. The efficiency of electricity production is about 28…30%, and the global efficiency of the electricity and thermal energy combined production, is about 75…78% (for the exhaust gases temperature of 90°C). Some of the advantages of the gas turbine units are the very low polluting emissions, without chemical treatment or afterburning; one single element in motion - the impeller; air bearings; cooling with air; the possibility to use a great variety of liquid and gaseous fuels, including gases with a high content of hydrogen sulphide (H_2S).

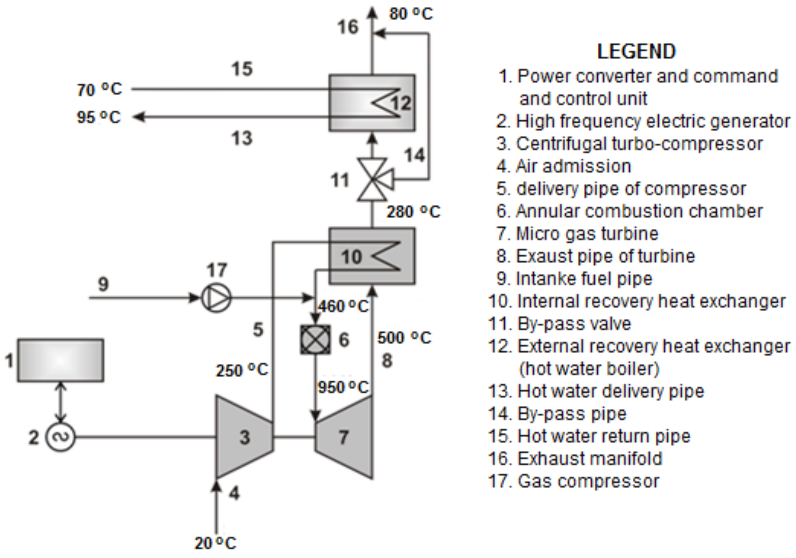

Fig. 4 − Operating scheme of a micro gas turbine cogeneration unit.

It is important to be mentioned also: the optimization for permanent operation at full load (24x7); the ability to track the load variations of the consumer; working unattended and automatic; requirement for less space; maintenance at great intervals of time (about 8000 h) and guaranteed operation over 80000 h; low level of noise (60...70 dBA at distance of 1 m).

The main disadvantages of the use of micro gas turbine cogeneration units are their electric lower efficiency, and their price still high.

The low power cogeneration unit from scheme of Fig. 4 may be realized with micro gas turbine cogeneration units of MT 250 type (FLEX TURBINE™, 2014) with nominal electric power of 250 kW. The compression ratio is about 6; the value of internal efficiency of the compressor is about 80…85% and, the temperature of compressed air of about 250°C. The combustion chamber operates with a air excess ratio about 5…6, the exhaust gases having an oxygen content of about 15% and a very low content of polluting emissions. The output temperature from the combustion chamber is about 920…950°C. The rotation speed of the turbine-compressor group is very high: 65000...70000 rpm, the exhaust gas temperature is of about 500°C and the value of the internal turbine efficiency is about 85…90%. After the heat recovery exchanger, the temperature of the exhaust gases is about 280°C and the temperature of the compressed air is about 460°C, the value of the internal recovery rate being 0.7...0.8. The exhaust gases are crossing the hot water boiler, which prepares hot water at 70/95°C. The hot water boiler has on the gases side an electronic controlled pass valve, its thermal load being according to consumer needs. The overall efficiency of the micro gas turbine cogeneration unit is about 45%. The maximum gas flow obtained from water, about 170 m^3_N/h, may produce a thermal output of 725 kW and an electrical output of 435 kW. The primary energy ratio of this thermal energy supply system, coupled with a micro gas turbine cogeneration unit, will be:

$$PER = \frac{\dot{Q} + P_{electrical}}{\left(\dot{Q}_H^{HWB} - \dot{Q}_{cogen}\right)} \cdot \eta_{HWB} \tag{2}$$

where $\dot{Q}_{cogen}$, [kW] is the thermal output and $P_{electrical}$, [kW] is the electrical output of cogeneration unit, the rest of terms having the same semnification as into previous Eq. (1). Considering $\dot{Q}$ = 4000 kW and $\dot{Q}_H^{HWB}$ = 2180 kW as before, the obtained value is *PER* = 2.7. Peak load of the system is, in this case, only 1/3 of the maximum load to be covered. The obtained electricity exceeds the needs of the circulation pumps and can be locally used. For a better flexibility, it is advantageous to install multiple units of lower power (two units of 250 kW or multiple units of 100 kW each). The cost of gas micro turbine cogeneration units is about to 700...800 EUR/kW of electricity, making investment in this case to recover quickly. The maintenance costs are very low, at 0.5...0.7 EUR/h, and the staff are virtually nil, because operation is completely automatic.

4.2. The Recovery of the Combustion Potential of the Gases Using Gas Engine Cogeneration Units

This kind of cogeneration implies the existence of one or more internal combustion engines, using as fuel the gases separated form geothermal water, connected to an electric generator. The thermal energy is produced by cooling the exhaust gases, lubricating oil and engine jacket.

Some advantages of the gas engine cogeneration are: much simpler systems, less voluminous, cheaper and fully controlled; the possibility of a large range of cogeneration (from some kW to more than 20 MW); a simple operation; a quick start with a short time constant (about 30 s to attain the nominal regime); this kind of cogeneration units can be located in the vicinity of energy consumers, resulting small losses in transport lines.

The main disadvantage of using gas engines is related to their vibrations and noise (about 100-120 dBA); this fact involves the use of silencers on the intake and the delivery lines, as well as a special mounting on heavy supports.

The gas engine cogeneration units can be integrated into a centralized heat supply network, or used – like in this case - for covering the local thermal needs; the generated electrical energy can be used for local needs and/or for the public grid. It is important to mention that the global efficiency of such a system is about 90%, greater than a system using micro gas turbines.

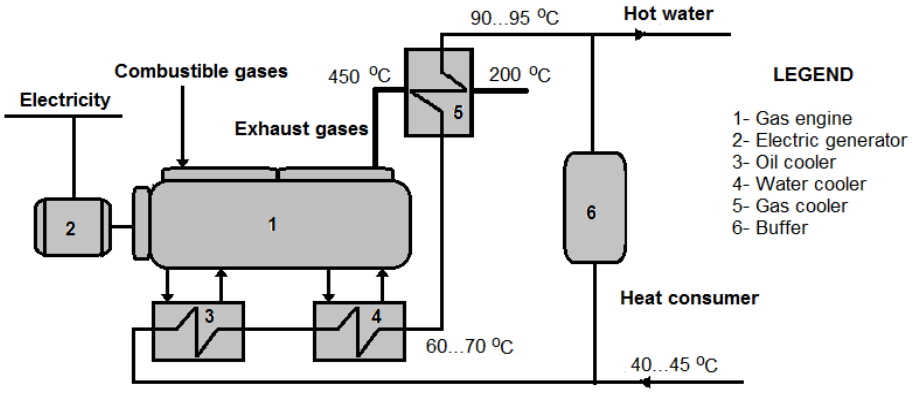

Fig. 5 − Operating scheme of a gas engine cogeneration unit.

The Fig. 5 presents the operating scheme of a gas engine cogeneration unit. The water returned from heating system, takes the heat from the engine lubrication system and cooling system, its temperature rising about to 60...70°C. The exhaust gases, having a temperature of about 450°C, warm up the water to a temperature of 90...95°C. The implementation of such a unit, into the geothermal station operating scheme, corresponds to Fig. 3. The maximum gas flow collected from well #1009 - Călimăneşti, about 170 m^3_N/h, may produce a

thermal output of 725 kW and an electrical output of 580 kW. The produced electricity, more much than in case of a microgas turbine unit, also exceeds its own consumption of the plant, and can be injected in local public grid. The primary energy ratio of this thermal energy supply system, coupled with a gas engine cogeneration unit, will be in accordance with Eq. (2) *PER* = 2.82, slightly larger than in the case of a micro gas turbine unit, due to higher electrical efficiency. This solution can be realized modular with small units; it results an economic and flexible system operation in according to thermal need of the consumer.

The cost of the gas engine cogeneration units is nowadays about 600…700 EUR/kW of electricity, which makes the investment to recover also quickly, and determines a low cost for the energy delivered in system. Such solution ensures energy independence, the cost of delivered energy including only the cost of geothermal water (imposed by the drill owner) and the cost for maintenance and operation. Compared with micro gas turbine cogeneration units, maintenance and operation costs are much higher, requiring permanent and qualified staff.

4.3. The Recovery of the Combustion Potential of the Gases Using Molten Carbonate Fuel Cell Cogeneration Units

The stationary power generation with Molten Carbonate Fuel Cell (MCFC) technology offers an efficient alternative to conventional fired power plants. It is considered as an intermediate temperature fuel cell as it operates at a temperature higher than polymer electrolyte fuel cell but lower than traditional solid oxide fuel cells, typically at 650°C. The high operating temperature serves as a big advantage for the MCFC. This leads to higher efficiency, since breaking of carbon bonds occurs much faster at higher temperatures. Other advantages include the flexibility to use more types of fuels and the ability to use inexpensive catalysts. Its ability to work with the different fuel types such as hydrogen, natural gas, light alcohols and its operation without noble metal catalysts, distinguishes it from low temperature fuel cells. A major disadvantage of MCFCs is that high temperatures enhance corrosion and the breakdown of cell components. Over the last five decades the MCFC technology has made impressive progress and a number of MCFC based power generators are currently in operation across the world. With the years of academic and industrial researches and developments in various countries such as USA, Japan, Korea and EU, the MCFC technology is approaching mass commercialization and MCFC is now the leader in terms of the number of installed power generation units among all fuel cell technologies (Kulkarni and Giddey, 2012).

The proposed layout consists in a hybrid scheme that integrates a high temperature MCFC and a gas turbine group. These hybrid systems are

particularly suitable to stationary power generation in the field of micro-cogeneration. The layout is presented in Fig. 6, which includes the temperature levels and highlights the electrical and thermal outputs. The mass-flow and energy rates were determined starting from the available methane volume flow rate about of 170 m^3_N/h and the corresponding available energetic potential of 1476 kW, as stated in Table 3.

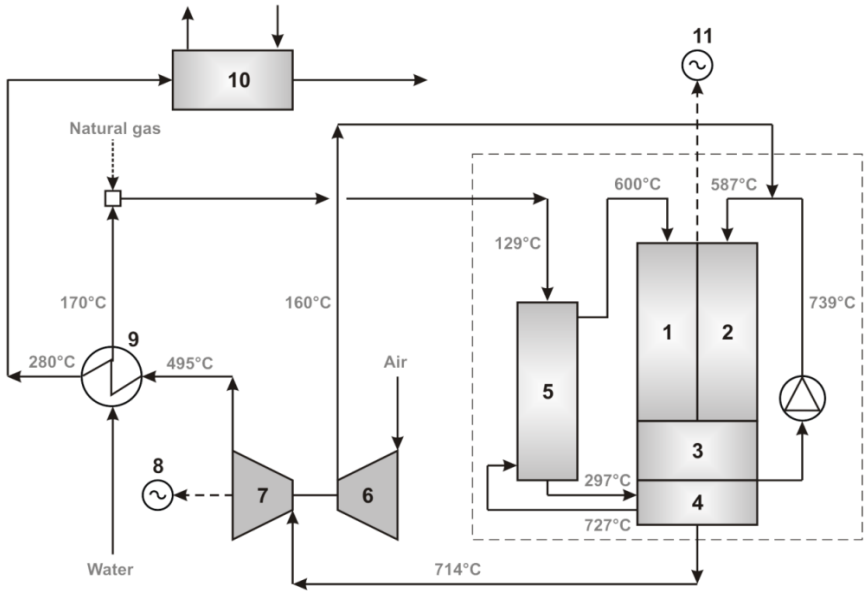

Fig. 6 − Molten carbonate fuel cell – gas turbine cogeneration system
1-anode; 2-cathode; 3-catalytic burner; 4-reformer; 5-regenerative heat exchanger; 6-air compressor; 7-gas turbine; 8-electric generator; 9-gas-water heat exchanger; 10-cogeneration heat exchanger; 11-electrical energy from fuel cell.

The cogeneration system will provide 716 kW electrical power from the MCFC stack, 94 kW electrical power from the GT bottoming cycle and 306 kW thermal power (at the cogeneration heat exchanger). We considered a bottoming cycle efficiency of 12.4% (Fermeglia *et al*., 2005), using the expression (De Simon *et al*., 2003):

$$\eta_{bc} = \frac{P_{turbine} - P_{compressor}}{P_{chemical} - P_{stack}} \tag{3}$$

The low value of the bottoming cycle (GT) efficiency is due to the fact that the operating pressure of 3.5 bar and the inlet turbine gas temperature, less than 700°C, are optimised for fuel cells stack and not for bottoming gas turbine cycle. The electrical efficiency can be expressed by formula:

$$\eta_{el} = \frac{P_{electrical}}{P_{chemical}} = \frac{P_{turbine} + P_{stack}}{P_{chemical}} \tag{4}$$

and the cogeneration efficiency by formula:

$$\eta_{cogen} = \frac{P_{electrical} + \dot{Q}_{cogen}}{P_{chemical}} \tag{5}$$

The chemical energy rate introduced with input methane based on lower heating value of the gas-flow rate is about 1476 kW, which leads to the values of the electrical efficiency about 55% and the cogeneration efficiency about 76%. The primary energy ratio of this thermal energy supply system, coupled with a MCFC, will be in accordance with Eq. (2): *PER* = 2.86, slightly larger than in the case of a gas engine unit, respectively micro gas turbine unit, due to very high electrical efficiency. The cost of MCFC cogeneration units is still high, about 2000 EUR/kW, up to three times higher than gas engine or micro gas turbine cogeneration units of same power. Manufacturers believe that the entry price where fuel cells could compete successfully with other small power generators would have to be roughly half of the current price (EPA, 2013).

5. Conclusions

The gases contained in geothermal water have an important thermal potential, which actually is not used. It is very difficult to find permanent local consumers due the fluctuating flow, caused by geothermal water use. The problem can be solved by using a low power cogeneration unit; in this way it is possible to obtain, in same time, additional thermal energy, and electricity which covers the entire electricity demand of the heating system. It was analyzed the using of three types of cogeneration plants functioning with the gases separated from geothermal water: micro gas turbine cogeneration unit, reciprocating gas engine unit and molten carbonate fuel cell unit. In none of these cases, the amount of gas was not sufficient to cover the total load of the heating system with additional thermal energy produced: as a result, in peak situations, it is necessary to use oil-fired boilers. Even in these conditions, it is highlighted a significant increase in effectiveness of the heating system: from *PER* = 1.65 when only geothermal energy is used, at *PER* = 2.7...2.9 in case of recovery the thermal potential of gases with a low power cogeneration plant.

Table 4
The Average Costs for Low Power Cogeneration Units in EUR/kW-Electrical Power

Cogeneration unit type	Equipment	Installation	Engineering/ contingency	Total
Reciprocating Gas Engine	810	365	390	1565
Micro Gas Turbine	1090	695	380	2165
Fuel Cell	4940	1430	130	6500

Current average costs for equipment, installation, design, engineering and management are shown in Table 4 (Santech, Inc., 2010).

Spark ignited gas engines are available in a wide range of sizes and offer low first cost, easy start-up, proven reliability when properly maintained, and good load-following characteristics. Gas engines have dramatically improved their performance and emissions profile in recent years. But maintenance and operation costs are higher, requiring permanent and qualified personnel.

Micro turbine systems are capable of producing power at around 25-33 percent efficiency by employing a heat exchanger that transfers exhaust heat back into the incoming air stream. The systems are air cooled and some designs use air bearings, thereby eliminating both water and oil systems used by reciprocating engines. Low emission combustion systems are being demonstrated and the potential for reduced maintenance and high reliability and durability are the basic advantages of these units.

Fuel cells produce power electrochemically and are generally more efficient than using fuel to drive a heat engine to produce electricity. Fuel cell efficiencies is upwards of 60% for MCFC. Fuel cells are inherently quiet and have extremely low emissions levels as only a small part of the fuel is combusted. The equipment and installations costs are still high, but the producers promise that by 2030 these costs become competitive with those of micro-turbines and gas engines. In these conditions, MCFC is a particularly cogeneration system, both in terms of efficiency and in terms of environmental impact.

The thermal potential of gases from geothermal water of the well #1009 can provide the functioning of cogeneration plant in the power range of 200...300 kW. The choosing a solution or the other depends on energy policy, market conditions and environmental policy in the moment of implementation decision.

RFERENCES

Antal C., Roşca M., *Current Status of Geothermal Development in Romania*, Proceedings of the 30-th Anniversary Workshop, UN University, August 26-27, Reykjavík, Iceland (2008) (Available on www.os.is).

Bianchi A.M., Dimitriu S., Băltăreţu F., *Solutions for Updating the Urban Electric Power and Heat Supply Systems, Using Geothermal Sources*, Termotehnica, An XV, **2**, 49-60 (2011).

Burchiu N., Burchiu V., Gheorghiu L.: *Centralized Heat Supply System Based on Geothermal Resources in the City of Călimăneşti - Valcea County* (in Romanian), Proceedings of the 4-th National Conference of Hydropower Engineers from Romania - Dorin Pavel, Paper Nr. 3.10, Bucharest (2006).

De Simon G., Parodi F., Fermeglia M., Taccani R., *Simulation of Process for Electrical Energy Production Based on Molten Carbonate Fuel Cells,* Journal of Power Sources, **115**, 210-218 (2003).

Entchev E., Yang L., Szadkowski F., Armstrong M., Swinton M., *Application of Hybrid Micro-Cogeneration System − Thermal and Power Energy Solutions for Canadian Residences,* Energy and Buildings, **60**, 345-354 (2013).

Fermeglia M., Cudicio A., De Simon G., Longo G., Pricl S., *Process Simulation for Molten Carbonate Fuel Cells*, Fuel Cells, **5**, *1*, 66-79 (2005).

Kulkarni A., Giddey S., *Materials Issues and Recent Developments in Molten Carbonate Fuel Cell,* Journal of Solid State Electrochemistry, **16**, *10*, 3123-3146 (2012).

Marasescu D., Mateiu A., *The Exploitation of the Potential of Low Enthalpy Geothermal Resources for Heating Supply of Localities,* ISPE Bulletin, **57**, *2*, 13-27 (2013).

Østergaard P.A., Lund H., *A Renewable Energy System in Frederikshavn Using Low-Temperature Geothermal Energy for District Heating*, Applied Energy, **88**, 479-487 (2011).

Roşca G.M., Antal C., Bendea C.: *Geothermal Energy in Romania*, Proceedings of Word Geothermal Congress 2010, April 25-29, Bali, Indonesia (2010).

Roşca G.M., Antics M., *Numerical Model of the Geothermal Well Located at the University of Oradea Campus,* Proceedings of the 24-th Workshop on Geothermal Reservoir Engineering, Stanford University, January 25-27, Stanford, California, USA (1999).

*** ANRSC (National Authority of Regulating and Monitoring for Community Services of Public Utilities): *Data on the State of Energy Services* (in Romanian), Website www.anrsc.ro .

*** EPA (Environmental Protection Agency), Office of Wastewater Management: *Renewable Energy Fact Sheet - Fuel Cells*, EPA (US) 832-F-13-014 (2013).

*** European Commission-Directorate General for Energy: *Renewables Make the Difference*, Publications Office of the EU, Luxembourg (2011).

*** FLEX TURBINE™, *Technical Specification MT250 Series Micro Turbine,* Website www.flexenergy.com.

*** ICEMENERG (National Research and Development Institute for Energy): *Study on Assessing the Current Energy Potential of Renewable Energy in Romania* (*Solar, Wind, Biomass, Micro Hydro, Geothermal*), *to Identify the Best Locations for Development Investment in Unconventional Electricity* (*in Romanian*), Ministry of Research Study for Economy, Bucharest (2006).

*** Romanian Government: HG 1535/2003 - *Decision Approving the Strategy for the Use of Renewable Energy*, Official Journal of Romania, **8**, January 07, Bucharest (2004).

*** SANTECH Inc., *Commercial and Industrial CHP Technology – Cost and Performance Data Analysis for EIA*, Report for US Energy Information Administration (2010).

SOLUŢII MODERNE PENTRU VALORIFICAREA POTENŢIALULUI ENERGETIC AL GAZELOR COMBUSTIBILE DIN APELE GEOTERMALE PRIN COGENERARE DE MICĂ PUTERE

(Rezumat)

Lucrarea are ca obiectiv analizarea posibilităţilor de valorificare a potenţialului termic al gazelor combustibile separate din apa geotermală furnizată de forajele aflate în exploatare pe valea Oltului, în perimetrul Călimăneşti – Căciulata – Cozia, concentrându-se pe staţia geotermală care furnizează energie termică sistemului de încălzire centrală al oraşului Călimăneşti. Utilizând un debit maxim de 10 l/s de apă geotermală furnizată de sonda nr. 1009 situată în vecinătate, staţia geotermală acoperă complet necesarul de energie termică pentru prepararea apei calde de consum şi cca 1/3 din sarcina maximă a sistemului centralizat de încălzire, restul fiind asigurat din surse clasice – cazane cu combustibil lichid. Debitul total al sondei fiind de 18 l/s, rezultă un debit maxim de gaze combustibile de cca. 170 m^3_N/h, reprezentând un potenţial termic brut de cca. 1,5 MW.

Lucrarea propune pentru utilizarea acestui potenţial o soluţie modernă, utilizând unităţi de cogenerare de mică putere, în domeniul de putere electrică 200...300 kW. S-au avut în vedere trei tipuri de astfel de unităţi, comercializate în mod curent: cu micro turbine cu gaze, cu motoare cu argere internă cu gaz şi cu pile de combustie cu carbonaţi topiţi. S-au trecut în revistă cele trei tipuri de unităţi de cogenerare, punându-se în evidenţă avantajele şi dezavantajele fiecăruia şi s-au stabilit performanţele sistemului actual, în ipoteza cuplării cu o astfel de unitate de cogenerare, utilizând drept combustibil gazele separate din apa geotermală. Se scoate în evidenţă faptul că pe lângă mărirea fluxului de căldură, introdus în sistemul centralizat de încălzire din surse regenerabile, se obţine şi acoperirea totală a necesarului de energie electrică pentru funcţionarea acestuia.

Analizând costurile actuale pentru echipamente, instalare şi M&O în fiecare din cazurile analizate se constată că la ora actuală soluţiile competititive sunt microturbinele cu gaze şi motoarele termice cu gaze. Pila de combustie este o soluţie deosebită atât din punct de vedere energetic cât şi din punct de vedere al impactului asupra mediului, dar costurile echipamentelor sunt încă deosebit de ridicate. Pila de combustie rămâne o soluţie preferată pentru viitor, producătorii promiţînd o importantă reducere a costurilor în următorii ani.

Autorii recomandă în final cuplarea sistemului actual de încălzire, bazat pe energie geotermală, cu cogenerare de mică putere realizată cu unităţi cu microturbine cu gaze sau motoare termice cu gaz, acestea putând funcţiona în condiţii de sarcină variabilă, obţinându-se o creştere a eficacităţii sistemului (PER) de cca 70%. Se estimează că investiţia poate fi recuperată într-o perioadă de cca 5-7 ani, ceea ce face ca această soluţie să fie interesantă.

BULETINUL INSTITUTULUI POLITEHNIC DIN IAŞI
Publicat de
Universitatea Tehnică „Gheorghe Asachi” din Iaşi
Volumul 62 (66), Numărul 1, 2016
Secţia
CONSTRUCŢII DE MAŞINI

THERMAL CONDUCTIVITY OF NANOFLUIDS BASED ON γ-Fe_2O_3 NANOPARTICLES

BY

GABRIELA HUMINIC[1,*], ANGEL HUMINIC[1], FLORIAN DUMITRACHE[2] and CLAUDIU FLEACA[2]

[1]Transilvania University of Braşov, Romania
Mechanical Engineering Department
[2]National Institute for Laser, Plasma and Radiation Physics, Măgurele, Romania
Laser Department

Received: May 7, 2015
Accepted for publication: May 25, 2015

Abstract. Thermal conductivity of γ-Fe_2O_3 nanofluid is reported by few researchers. The current study is focused on the measurement of thermal conductivity of the γ-Fe_2O_3nanoparticles dispersed in distilled water. Experiments were performed for four the weight concentrations 0.5%, 1.0%, 2.0% and 4.0% respectively and the temperature in range 25°C to 50°C. The experimental results were compared to theoretical models and experimental data available in literature.

Keywords: nanoparticles; nanofluids; thermal conductivity.

1. Introduction

The magnetic fluids have remarkable potential for engineering applications being used in different fields such as thermal engineering, electronic packing and bioengineering (Rosensweig, 1985; Odenbach, 2002). Magnetic nanoparticles used in magnetic nanofluids are usually prepared in different sizes and morphologies from metal materials (ferromagnetic materials) such as iron, cobalt, nickel as well as their oxides (ferromagnetic materials)

[*]Corresponding author; *e-mail*: gabi.p@unitbv.ro

such as maghemite (Fe_2O_3), magnetite (Fe_3O_4), spinel-type ferrites, etc. (Nkurikiyimfura *et al*., 2013).

In the last decade, researchers are focusing on the measurement of thermal conductivities and viscosities of magnetic fluids in the absence or presence of magnetic fields, because of the unique magnetic properties of these nanofluids (Syam Sundar *et al*., 2013a; Syam Sundar *et al*., 2013b; Khedkar *et al*., 2013; Yu *et al*., 2010; Abareshi *et al*., 2010; Hong *et al*., 2006).

In the work (Syam Sundar *et al*., 2013a) the authors measured the thermal conductivity and viscosity of water based magnetite (Fe_3O_4) nanofluid as a function of particle volume fraction at different temperatures. Their results showed that the thermal conductivity ratio increased with the increase of particle volume fraction and increase of temperature. Maximum thermal conductivity enhancement of 48% was observed with 2.0% volume concentration at 60°C temperature compared to distilled water. Also, same authors (Syam Sundar *et al*., 2013b) investigated the thermal conductivity enhancement of the ethylene glycol and water mixture based magnetite (Fe_3O_4) nanofluids. Experiments were conducted in the temperature range from 20 °C to 60°C and in the volume concentration range from 0.2% to 2.0%.They found that the thermal conductivity for 20:80% EG/W based nanofluid is 46%, 40:60% EG/W based nanofluid is 42% and 60:40% EG/W based nanofluid is 33% at 2.0% particle volume concentration at a temperature of 60°C.

Khedkar (Khedkar *et al*., 2013) measured the thermal conductivity and viscosity of Fe_3O_4 nanoparticles in paraffin as a function of particle volume fraction. The experimental results showed that the thermal conductivity increases with an increase of particle volume fraction, and the enhancement observed to be 20% over the base fluid for a paraffin nanofluid with 0.1 volume fraction of Fe_3O_4 nanoparticles at room temperature.

The effects of particle volume fraction on the thermal conductivity of a kerosene based Fe_3O_4 magnetic nanofluid prepared via a phase-transfer method were investigated by Yu (Yu *et al*., 2010). Their results showed that the thermal conductivity ratios obtained increased linearly with the increase of volume fraction and temperature and the value was up to 34.0% at 1 vol%.

The thermal conductivity of a water based magnetite nanofluid as a function of particle volume fraction at different temperatures was measured by (Abareshi *et al*., 2010). The thermal conductivity increased with the increase of the particle volume fraction and temperature. The maximum thermal conductivity ratio was 11.5% at a particle volume fraction of 3% at 40°C.

Hong (Hong *et al*., 2006) investigated the thermal conductivity of nanofluids with different volume fractions of Fe nanoparticles in ethylene glycol. Their results confirmed the intensification of thermal conductivity with the particle volume fraction. In the comparison of the copper and iron nanoparticles dispersed in ethylene glycol, the thermal conductivity enhancement in iron- based nanofluids was higher than that in copper-based nanofluid.

The main goal of the present study is to investigate the effects of the temperature and of the weight concentration on thermal conductivity of γ-Fe_2O_3 /water nanofluids.

2. Experimental Procedure

2.1. Preparation of the Nanofluids

In this study, the nanofluids in 0.5, 1.0, 2.0 and 4.0 wt.% concentrations were prepared. 3,4-Dihydroxy-L-phenylalanine (L-DOPA) product no. D9628 was used as surfactants for γ-Fe_2O_3 nanoparticles. The concentration of surfactant for each type of nanofluid is 3g/l. In order to obtain homogeneous suspensions with size aggregates as small as possible was used a double ultrasonication: 10 h at Elmasonic S40H bath followed by 3 h under Hielscher UIP 1000hd sonotrode). In all cases we maintained a 70°C temperature during ultrasonication. No settlement of nanoparticles was observed after 6 months.

2.2. Thermal Conductivity Measurements

Thermal conductivity was measured using a KD 2 Pro thermal properties analyzer. The device consists of a probe with 1.3 mm in diameter and 60 mm in length, a thermo-resistor and a microprocessor to control and measure the conduction in the probe. The instrument has a specified accuracy of ±5%. Before measurements, the calibration of the sensor needle was carried out first by measuring thermal conductivity of distilled water.

Before measurements, the calibration of the sensor needle was carried out first by measuring thermal conductivity of distilled water and glycerin. Thus, the measured value for distilled water and glycerine were 0.600 W/mK and 0.287 W/mK respectively, which were in agreement with the literature values of 0.596 W/mK and 0.285 W/mK respectively at a temperature of 293K.

In order to maintain a prescribed constant temperature during the measurement process, a thermostat bath (Haake C10 - P5/U with an operating range of 25-100°C) was used with an accuracy of ±0.04°C.

3. Results and Discussions

Iron oxide nanoparticles have been characterized using TEM (transmission electron microscopy) analysis (Fig. 1). The iron oxide nanoparticles have two distinct features:

− the small nanoparticles are the most common, having a spherical shape, 5.5 nm mean diameter and are arranged in chain like superposed agglomerates;

− the big particles have polyhedral with round corners shape, are less agglomerated or cross-linked and their sizes vary between 12 to 20 nm.

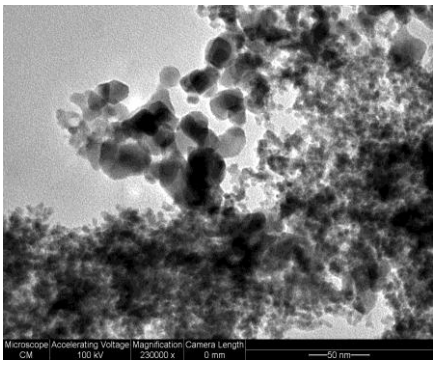

Fig. 1 − TEM image of iron oxide based sample.

In order to prevent particle aggregation and the obtain of the stable nanofluids in time different surfactants were used. Most used surfactants in the preparation of the nanofluids were sodium dodecylsulfate (SDS) (Zhou *et al*., 2012; Saleh *et al*., 2014; Haitao *et al.*, 2013; Hwang *et al*., 2007), sodium dodecylbenzenesulfonate (SDBS) (Zhou *et al*., 2012; Li *et al*., 2008; Zhu et *al.*, 2009; Wang *et al*., 2009) and salt and oleic acid (Yu *et al.*, 2009; Hwang *et al.*, 2008; Ding *et al*., 2007), cetyltrimethylammoniumbromide (CTAB) (Pantzali *et al*., 2009), polyvinylpyrrolidone (PVP) (Zhu *et al*., 2007). In this study, γ-Fe_2O_3/water nanofluids were mixed with L-DOPA surfactant. From our knowledge these surfactants were not used until present of researchers.

The thermal conductivity was measured for different temperature (25°C, 30°C, 35°C, 40°C, 45°C and 50°C) and various weight concentrations (0.1%, 0.5%, 1.0%, 2.0% and 4.0%). As it is observed in Fig. 2 the thermal conductivity ratio of nanofluids defines as the ratio of the thermal conductivity of the nanofluids and the thermal conductivity of the base fluid increases both with the temperature and the weight concentration of nanoparticles. A similar trend is observed by (Syam Sundar *et al.*, 2013a; Yu *et al*., 2010; Abareshi *et al*., 2010).

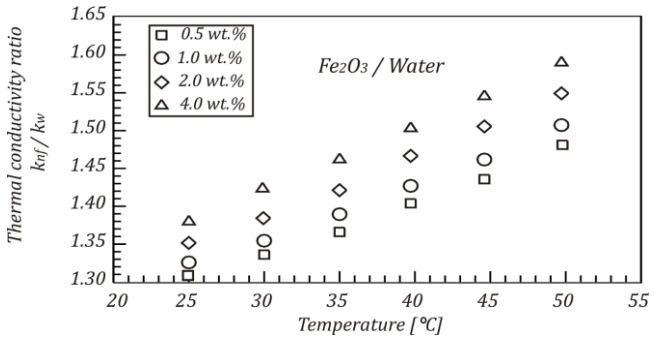

Fig. 2 − The thermal conductivity ratio versus temperature at different weight concentrations of γ-Fe_2O_3 nanoparticles.

Fig. 3 shows comparisons between the measured data and the predicted values using existing correlations from literature at 25°C. For the comparison experimental data concerning the thermal conductivity of γ-Fe_2O_3/water nanofluids were chosen two models: Murshed and Sundar models.

The model for predicting the effective thermal conductivity of nanofluids developed by (Murshed *et al.*, 2006) is:

$$k_{eff,Murshed} = \frac{k_{bf}\left[1+0.27\phi^{4/3}\left(\frac{k_s}{k_{bf}}-1\right)\right]\left[1+\frac{0.52\phi}{1-\phi^{1/3}}\left(\frac{k_s}{k_{bf}}-1\right)\right]}{1+\phi^{4/3}\left(\frac{k_s}{k_{bf}}-1\right)\left(\frac{0.52\phi}{1-\phi^{1/3}}+0.27\phi^{1/3}+0.27\right)} \quad (1)$$

Recently, Syam Sundar (Syam Sundar *et al.*, 2013a) has developed a new model to predict the effective thermal conductivity of nanofluids, valid for Fe_3O_4/ water nanofluids in the range $0 < \phi < 2.0$ vol.% and 20°C < *T* <60°C:

$$k_{eff,Syam\ Sundar} = k_{bf}\left(1+10.5\phi\right)^{0.1051} \quad (2)$$

where k_{bf} is thermal conductivity of base fluid, k_s − thermal conductivity of solid particles and ϕ − the volume concentration of nanoparticles.

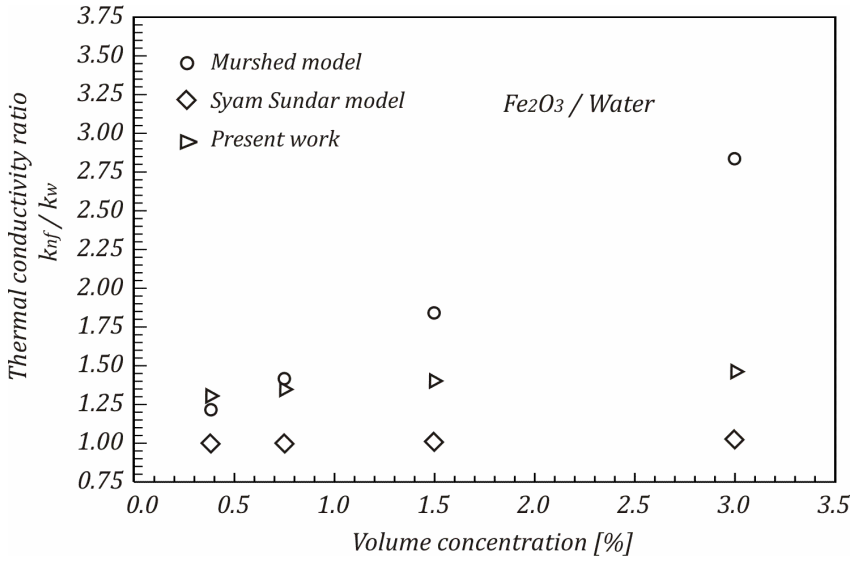

Fig. 3 − Comparison between experimental data and correlations available in literature.

As shown in Fig. 3, at lower volume concentrations of nanoparticles the experimental data were in agreement with Murshed model. The difference between our results and Sundar model can be explained by used different factors such as surfactant (in the Sundar model the used surfactant was Cetyl trimethyl ammonium bromide (C-TAB)), the particle size as well the preparation method.

4. Conclusions

In this paper, the thermal conductivity of nanofluids based on γ-Fe_2O_3 nanoparticles were experimentally investigated. Nanopowders were synthesized laser pyrolysis technique from iron pentacarbonyl vapors carried by ethylene who also acts as laser energy transfer agent. Their aqueous suspensions in presence of the additive L-DOPA were prepared by double ultrasonication. Thermal conductivities of γ-Fe_2O_3 nanoparticles in distilled water were determined experimentally as a function of weight concentration and temperature. The experimental results showed that the thermal conductivity of nanofluids is much higher than the thermal conductivity of base fluid. Also, the thermal conductivities of the γ-Fe_2O_3/water nanofluids increase linearly both with the weight concentration and the temperature.

Acknowledgements. This work was supported by a grant of the Romanian National Authority for Scientific Research, CNCS – UEFISCDI, Project Number PN-II-ID-PCE-2011-3-0275.

REFERENCES

Abareshi M., Goharshadi E., Zebarjad S.M., Fadafan H.K., Abbas Y., *Fabrication, Characterization and Measurement of Thermal Conductivity of Fe_3O_4 Nanofluids,* Journal of Magnetism and Magnetic Materials, **322**, 3895-3901, 2010.

Ding Y., Chen H., He Y., Lapkin A., Yeganeh M., Siller L., Butenko Y.V., *Forced Convective Heat Transfer of Nanofluids,* Adv. Powder Technology, **18**, 813-824, 2007.

Haitao Hu, Peng H., Ding G., *Nucleate Pool Boiling Heat Transfer Characteristics of Refrigerant/Nanolubricant Mixture with Surfactant,* International Journal of Refrigeration, **36**, 1045-1055, 2013.

Hong K.S., Hong T.K., Yang H.S., *Thermal Conductivity of Fe Nanofluids Depending on the Cluster Size of Nanoparticles,* Applied Physics Letters, **88**, 031901, 2006.

Hwang Y., Lee J.K., Lee C.H., Jung Y.M., Cheong S.I., Lee C.G., Ku B.C., Jang S.P., *Stability and Thermal Conductivity Characteristics of Nanofluids,* Thermochimica Acta, **455**, 70-74, 2007.

Hwang Y., Lee J.K., Jeong Y.M., Cheong S.I., Ahn Y.C., Ki S.H., *Production and Dispersion Stability of Nanoparticles in Nanofluids*, Powder Technology, **186**, 145-153, 2008.

Li X.F., Zhu D.S., Wang X.J., Wang N., Gao J.W., Li H., *Thermal Conductivity Enhancement Dependent pH and Chemical Surfactant for Cu–H_2O Nanofluids*, Thermochimica Acta, 469, 98-103, 2008.

Khedkar R.S., Sai Kiran A., Sonawane S.S., Wasewar K., Umre S.S., *Thermophysical Characterization of Paraffin Based Fe_3O_4 Nanofluids*, Procedia Engineering, 51, 342-346, 2013.

Murshed S.M.S., Leong K.C., Yang C., *A Model for Predicting the Effective Thermal Conductivity of Nanoparticle–Fluid Suspensions*, International Journal of Nanoscience, **5**, 23-33, 2006.

Nkurikiyimfura I., Wang Y., Pan Z., *Heat Transfer Enhancement by Magnetic Nanofluids - A Review,* Renewable and Sustainable Energy Reviews, **21,** 548-561, 2013.

Odenbach S., *Ferrofluids,* Springer, Berlin, 2002.

Pantzali M.N., Mouza A.A., Paras S.V., *Investigating the Efficacy of Nanofluids as Coolants in Plate Heat Exchangers* (*PHE*), Chem. Eng. Sci., **64**, 3290-3300, 2009.

Rosensweig R.E., *Ferrohydrodynamics*, Cambridge University Press, New York, U.S.A., 1985.

Saleh R., Putra N., Wibowo R.E., Septiadi W.N., Prakoso S.P., *Titanium Dioxide Nanofluids for Heat Transfer Applications,* Experimental Thermal and Fluid Science, **52**, 19-29, 2014.

Syam Sundar L., Singh Manoj K., Sousa Antonio C.M., *Investigation of Thermal Conductivity and Viscosity of Fe_3O_4 Nanofluid for Heat Transfer Applications,* International Communications in Heat and Mass Transfer, **44,** 7-14, 2013a.

Syam Sundar L., Singh Manoj K., Sousa Antonio C.M., *Thermal Conductivity of Ethylene Glycol and Water Mixture Based Fe_3O_4 Nanofluid,* International Communications in Heat and Mass Transfer, **49**, 17-24, 2013b.

Wang X.J., Zhu D.S., Yang S., *Investigation of pH and SDBS on Enhancement of Thermal Conductivity in Nanofluids,* Chem. Phys. Lett., **470**, 107-111, 2009.

Yu W., Xie H., Chen L., Li Y., *Enhancement of Thermal Conductivity of Kerosene-Based Fe_3O_4 Nanofluids Prepared via Phase-Transfer Method,* Colloids and Surfaces A: Physicochem. Eng. Aspects, **355**, 109-113, 2010.

Zhou M., Li G.X., Chai L., Zhou L., *Analysis of Factors Influencing Thermal Conductivity and Viscosity in Different Kinds of Surfactant Solutions*, Experimental Thermal and Fluid Science, **36**, 22-29, 2012.

Zhu D., Li X., Wang N., Wang X., Gao J., Li H., *Dispersion Behavior and Thermal Conductivity Characteristics of Al_2O_3–H_2O Nanofluids,* Curr. Appl. Phys., **9**, 131-139, 2009.

CONDUCTIVITATEA TERMICĂ A NANOFLUIDELOR BAZATE PE NANOPARTICULE DE γ-Fe_2O_3

(Rezumat)

Nanofluidele magnetice au un potenţial remarcabil pentru aplicaţii în inginerie şi medicină. În ultimul deceniu, cercetătorii s-au concentrat pe măsurarea conductivităţii termice, în absenţa sau prezenţa câmpurilor magnetice, datorită proprietăţilor magnetice unice ale acestor nanofluide. În acestă lucrare se prezintă un studiu referitor la conductivitatea termică a nanofluidelor γ-Fe_2O_3/apă. Conductivitatea termică a nanofluidelor a fost măsurată cu ajutorul aparatului KD 2 Pro a cărui principiu de măsurare se bazează pe metoda firului cald. Intervalul de temperatură în care conductivitatea termică a nanofluidelor a fost măsurată este cuprins între 25°C şi 50°C. De asemenea, conductivitatea termică a nanofluidelor γ-Fe_2O_3/apă a fost măsurată pentru diferite concentraţii masice (0.5%, 1.0%, 2.0% şi 4.0%) de nanoparticule. Rezultatele obţinute au scos în evidenţă că aceste nanofluide prezintă o conductivitate termică mult mai ridicată decât conductivitatea termică a apei. Raportul dintre conductivitatea termică a nanofluidelor şi conductivitatea termică a apei creşte semnificativ cu creşterea temperaturii şi, de asemenea, cu creşterea concentraţiei masice de nanoparticule. În final, rezultatele experimentale au fost comparate cu modelele teoretice şi datele experimentale disponibile în literatură.

BULETINUL INSTITUTULUI POLITEHNIC DIN IAŞI
Publicat de
Universitatea Tehnică „Gheorghe Asachi” din Iaşi
Volumul 62 (66), Numărul 1, 2016
Secţia
CONSTRUCŢII DE MAŞINI

THERMAL ANALYSIS OF A UNIVERSITY CAMPUS HEATING PLANT

BY

OANA ZBARCEA, FLORIN POPESCU[*] and ION V. ION

“Dunărea de Jos” University of Galaţi, Romania,
Department of Thermal Systems and Environmental Engineering

Received: April 25, 2015
Accepted for publication: May 30, 2015

Abstract. University campus buildings are high energy consumers, despite the fact that they have low operating periods during the holidays that coincide with periods of maximum energy consumption. These buildings are used for diverse activities (research, classrooms, offices, dormitories, libraries) by a variable number of people for different time periods. This study describes the thermal analysis of the buildings and the district heating system with natural gas boilers performed in order to identify the components with higher inefficiency and then to determine strategies for energy saving. The study revealed an energy saving potential of about 7%. The main strategies for thermal energy saving on campus are: increasing the efficiency of heating boilers, controlling indoor temperature design, and improving the thermal performance of buildings envelope. A future research direction will be to analyse the possible energy, environmental and economic gains by recovery of waste heat contained in flue gas exhausted by heating boilers.

Key words: heating plant; thermal analysis; university campus.

[*]Corresponding author; *e-mail*: florin.popescu@ugal.ro

1. Introduction

Worldwide, new heating technologies are turning our attention to energy efficiency, reduced fuel consumption, reduced water consumption and exhaust emissions. The European Union (EU) set the ambitious objective to reduce the greenhouse gas emissions by 20% till 2020 (http://ec.europa.eu/). As the energy consumption in buildings at European level is 40% of total energy consumption, it results that the greatest potential for energy conservation is found in buildings. Buildings in universities campuses, as well as hospitals, hotels, schools, commercial buildings are considered as energy-guzzling buildings, equivalent to buildings with an annual consumption of more than 2000 tonne oil equivalent/year (Min Hee Chung and Eon Ku Rhee, 2014). The buildings in universities campus have high energy consumption because they are used for diverse activities (research, classrooms, offices, dormitories, libraries) and are also used by a variable number of people for different time periods. The energy consumption of these buildings should have lower energy consumption due to holidays overlap with periods in which heating or cooling demand is the highest. More studies have been conducted regarding energy conservation in universities campuses and various strategies have been proposed such as: improving administrative policies, using automatic metering systems, using of high efficient energy equipment, implementing energy conservation technologies and renewable energy systems (Min Hee Chung and Eon Ku Rhee, 2014; Nurdan Yildirim, 2006).

This study attempts to analyse the potential for energy conservation only in the heating system of "Dunărea de Jos" campus, excluding buildings, since most of them are old and have already been upgraded in recent years, new windows, doors and roofs being changed.

From this perspective, energy conservation strategies may include: increasing the efficiency of heating boilers, implementing a system for controlling indoor temperature and thermal insulation of buildings.

2. University Campus Presentation

The main campus of "Dunărea de Jos" University consists of 22 buildings with different characteristics and different utilization (Fig. 1). The total floor area is 17027 m^2 and the heat load (according to the natural gas bills) in the last heating season was 6165956.99 kW. The buildings are heated by a district heating system with 3 (similar) natural gas boilers. The buildings characteristics are given in Table 1 and the heating boilers characteristics are given in Table 2.

The main components of the heating system are distributed in (1) heating boilers building, (2) heat exchanger building, (3) pipe lines between

these two buildings, (4) pipe lines for hot water distribution to buildings (consumers) and (5) circulation pumps.

The hot water from boilers flows to the heat exchanger where transfers a part of its heat to the water for buildings heating (consumers).The water is redirected towards the consumers through 4 main pipes; each pipe having a number of buildings that need to be heated.

Table 1
Building Characteristics

Building code	Building type	Volume [m^3]	Total floor area, [m^2]	Number of floors	Orientation	Wall	
						Materials	Thickness [cm]
Y	Educational	48240	1.206	7	V	Concrete	30
G	Educational	11907	756	4	S	Concrete	30
I	Workshop	1874	310.8	0	E	Sandwich panels	10
E	Educational	10706	874	3	E	Concrete	30
L	Educational	6344	83807	1	E	Concrete	30
CN	Laboratories	3520	465	1	V	Brick	30
K	Laboratories	5388	857	2	S	Concrete	30
F	Educational	8949	885	2	E	Concrete	30
D	Educational	11340	1073	1	E	Concrete	30
B	Educational	8470	711	2	V	Concrete	30
H	Workshop	7614	1015	0	V	Concrete	30
P	Thermal point	2523	650	1	S	Concrete	30
SA	Educational	3006	288	1	E	Concrete	30
SB	Educational	8118	447	4	E	Concrete	30
SC	Educational	3194	398	0	E	Concrete	30
SD	Educational	11177	507	5	E	Concrete	30
SE	Educational	3279	292	1	N	Concrete	30
AN	Educational	16788	1492	2	V	Brick	30
AE	Educational	9926	88235	2	E	Brick	30
AS	Educational	12233	1087	2	S	Brick	30
AR	Educational	1477	19514	1	V	Brick	30
J	Workshop	6952	1137	0	N	Concrete	30

Table 1
Continuation

Building code	Roof type	Insulation	
		Materials	Thickness [cm]
Y	Mansard	Default	
G	Hipped	Default	
I	Flat	Mineral wool	10
E	Flat	Default	
L	Hipped	Default	
CN	Flat	Default	
K	Hipped	Default	
F	Flat	Default	
D	Flat	Default	
B	Flat	Default	
H	Flat	Default	
P	Flat	Default	
SA	Flat	Default	
SB	Flat	Default	
SC	Flat	Default	
SD	Flat	Default	
SE	Flat	Default	
AN	Hipped	Default	
AE	Hipped	Default	
AS	Hipped	Default	
AR	Hipped	Default	
J	Flat	Default	

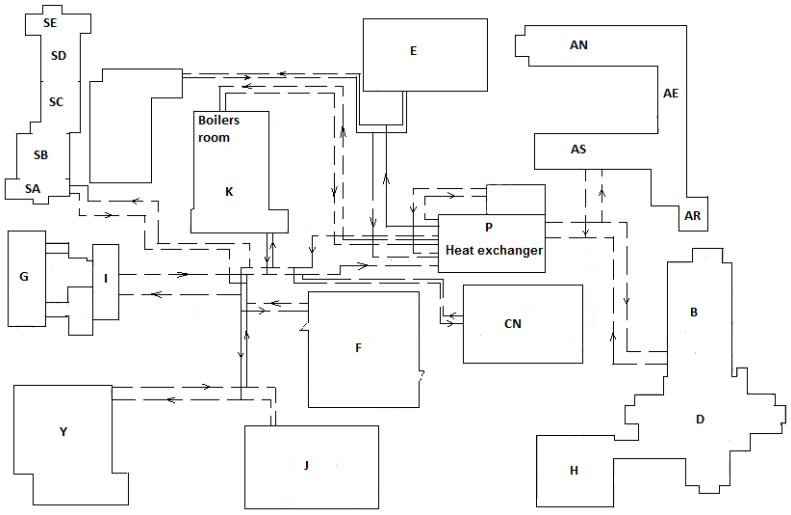

Fig. 1 − "Dunărea de Jos" University campus.

Table 2
Heating Boilers Characteristics

Net power / boiler	kW	2000
Efficiency at 100%	%	95.51
Efficiency at 30%	%	95.80
Maximum flue gas flow rate	m^3/h	3301.69
Flue gas temperature	°C	184
Pressure drop water circuit	mbar	25
Normal pressure	bar	5
Total capacity	l	2000
Electric power	W	20
Fuel type	–	natural gas

The pressure in the installation is set to 2.33 bars. The heating boilers are similar and have three levels of combustion control. The temperature of hot water is set at 70°C and the temperature of return water is set at 55°C. The heating system should provide a constant temperature of 21°C in buildings.

The heating boilers are fully automatized. They stop when the outside temperature reaches 20°C.

3. Thermal Analysis of Heating System

The heating system analysis started with calculation of energy consumption for heating according to the Methodology for calculation of buildings energy performance – Mc001-2006 (http://www.mdrl.ro/), developed based on European standards.

The seasonal energy consumption for heating is given by the following general equation:

$$Q_{f,h} = \left(Q_h - Q_{rhh} - Q_{rwh}\right) + Q_{th}, \text{ [kWh]} \quad (1)$$

where: Q_h – energy demand for building heating, [kWh]; Q_{rhh} – heat recovered from the heating plant, [kWh]; Q_{rhw} – heat recovered from the preparing of domestic hot water and used for building heating, [kWh]; Q_{th} – total heat loss of the heating plant, [kWh].

The seasonal energy consumption for heating was also calculated by using the software given in (http://vl.academicdirect.ro/), which calculates in simplified way the heating demand considering several parameters such as: characteristics of walls, windows, roof, floor and environmental temperatures. The results of calculations are given in Table 3.

Table3
Heat Demand Calculation Results

Heat demand, [kWh]	First method	Second method
	5812239.59	5922118.98

It can be seen that there is a difference of about 1.5% between the results obtained using the calculation methodologies.

The real energy consumption for buildings heating was calculated by summing the monthly natural gas consumption during the period of 1st of October 2014 and 31st of March 2015 (Table 4).

Comparing the data given in Table 3 and Table 4 it can be noted that the real energy consumption for heating is higher with 7.24% than the calculated energy demand. The difference represents the heat losses associated to heating boilers, heat exchanger and hot water pipe lines.

Table 4

Registered Consumption of Natural Gas

Consumption period	Natural gas consumption [kWh]
1st of October 2014 – 31st of March 2015	6265958.99

4. Conclusions

The study results show an energy saving potential in the heating system, without energy modernisation of buildings, of about 7%. The main strategies for thermal energy saving on campus include increasing the efficiency of heating boilers, controlling indoor temperature design, and improving the thermal performance of buildings envelope. A future research direction will be to analyse the possible energy, environmental and economic gains by recovery of waste heat contained in flue gas exhausted by heating boilers. The average measured exhaust temperature of flue gas is about 170°C. An especial attention will be paid to application of water preheating in a condensing economizer as an alternative for the consumption of natural gas in boilers for university buildings heating. This is a solution that has been demonstrated successfully for many boiler applications (Gas Technology Institute, 2013).

REFERENCES

Min Hee Chung, Eon Ku Rhee, *Potential Opportunities for Energy Conservation in Existing Buildings on University Campus: A Field Survey in Korea*, Energy and Buildings, **78**,176-182 (2014).

Nurdan Yildirim, Macit Toksoy, Gulden Gokcen, *District Heating System Design for a University Campus*, Energy and Building, **38**, 1111-1119 (2006).

http://vl.academicdirect.ro/molecular_dynamics/heating_buildings/form.php

** Gas Technology Institute, *Energy and Water Recovery with Transport Membrane Condenser*, Study CEC-500-2013-001, January 2013.

** *Metodologia de calcul privind performanţa energetică a clădirilor* Mc001–2006 (http://www.mdrl.ro/_documente/constructii/reglementari_tehnice/Anexa1_Ordin1071.pdf).

[*] *The 2020 Climate and Energy Package*, http://ec.europa.eu/clima/policies/package/index_en.htm

ANALIZA TERMICĂ A CENTRALEI TERMICE DINTR-UN CAMPUS UNIVERSITAR

(Rezumat)

Tehnologiile din sectorul energetic evoluează în permanenţă, iar atenţia se îndreaptă spre eficientizarea şi optimizarea sistemelor de încălzire pentru reducerea consumului de combustibil, a pierderilor de căldură şi creşterea randamentului centralelor termice. Uniunea Europeană şi-a propus un obiectiv ambiţios de reducerea emisiilor de gaze cu efect de seră cu 20% până în 2020, iar un pas important în această direcţie este reducerea consumului de combustibili fosili necesar încălzirii clădirilor. În categoria clădirilor mari consumatoare de energie se regăsesc şcolile, spitalele, hotelurile, clădirile cu destinaţie comercială şi clădirile din campusurile universitare.

În alte studii de specialitate s-au atins subiecte precum îmbunătăţirea politicilor administrative, utilizarea de echipamente de încălzire cu eficienţă energetică ridicată sau utilizarea sistemelor energetice regenerabile.

Acest studiu descrie analiza termică a clădirilor şi a sistemului de încălzire cu gaze naturale dintr-un campus universitar pentru a determina strategiile de utilizare mai eficientă a sistemului. Pe baza rezultatelor s-a stabilit că există un potenţial de economisire a energiei de aproximativ 7%, dacă se iau o serie de măsuri precum creşterea eficienţei cazanelor, automatizarea sistemului de control a temperaturii interioare fără a considera îmbunătăţirea performanţelor energetice ale clădirilor.

În cercetările viitoare se vor analiza posibilităţile de îmbunătăţire a sistemului de încălzire prin preîncălzirea apei într-un economizor cu condensare.

BULETINUL INSTITUTULUI POLITEHNIC DIN IAŞI
Publicat de
Universitatea Tehnică „Gheorghe Asachi” din Iaşi
Volumul 62 (66), Numărul 1, 2016
Secţia
CONSTRUCŢII DE MAŞINI

EXPERIMENTAL CHARACTERIZATION OF MATERIALS SUBJECTED TO COMBINED LOADINGS PART I: TENSION-TORSION

BY

LIVIU ANDRUŞCĂ*

"Gheorghe Asachi" Technical University of Iaşi, Romania,
Department of Mechanical Engineering, Mechatronics and Robotics

Received: January 8, 2016
Accepted for publication: March 10, 2016

Abstract. This paper presents a set of experimental characterizations for materials subjected to different loading paths. The methodology consists in testing circular specimens by tension-torsion combined loadings. Tensile initial loadings are stopped when different values of extension are achieved. Subsequently torsion loads are applied until specimens fails. Experimental results shows that hardness and Young modulus decrease when extension decreases. Subsequent loading by torsion has a significant influence on material final microstructure for each of six cases.

Keywords: complex loading paths; fractographical examination; instrumented indentation tests.

1. Introduction

Materials are subjected to a complex historic of loading and deformation during exploitation. To obtain multiaxial stress states in laboratory conditions different experimental procedures can be applied: biaxial tensile tests (Andruşcă *et al*., 2015a), combined loadings (Andruşcă *et al.*, 2015b) etc.

*Corresponding author; *e-mail*: liviu.andrusca@tuiasi.ro

Severe plastic deformation represents an effective method to obtain ultrafine grained (UFG) and nanocrystalline materials which consists in combining torsion, tension or/and compression loads (Wang *et al.*, 2014). Experiments under combined axial and torsion loads are used to evaluate ductile failure (Haltom *et al.*, 2013; Graham *et al.*, 2012), to obtain initial and subsequent yield surfaces under different tension-torsion loading paths (Hu *et al.*, 2012), to study inhomogeneous plastic deformations (Khoddam *et al.*, 2014), to study micro-structural evolution of pure copper (Li *et al.*, 2014). Instrumented indentation tests (ISO 14577-1) are used to assess evolution of materials characteristics at several levels of deformation. For materials with ductile behavior one of the most important parameters is the yield stress. Another important feature of combined loadings is represented by the study of rupture mechanisms in combined tension and shear. Failure mechanisms are governed by internal necking mechanism and internal shearing mechanism (Barsoum *et al.*, 2007). The transition from internal necking (tensile load) to internal shear (torsion load) can be connected with the variation range (high to low) of stress triaxiality (Barsoum *et al.*, 2011).

2. Material and Methods

To characterize material behavior are used two approaches: macroscopic (combined loading) and microscopic (SEM analysis and nano-indentation tests). This study is focused on microscopic approach. Two successive different loading paths were performed: initial tension combined with subsequent torsion and initial torsion followed by subsequent tension. In this study experimental procedure of combined loadings assumes the next cycle: tensile preloading-elastic recovery- torsion reloading until break.

Initial loading of circular specimens in the case of combined loading analysed in this paper was tension. Uniaxial tensile test are performed on a universal testing machine Intron 8801. The subsequent loading was torsion. Torsion tests are performed through an attachable device that allows free end torsion. SEM technique is used to analyze failure surfaces and to investigate microstructural changes. From failed circular specimens small disc pieces are cuted near from the vicinity of the rupture zone. On this discs is determined hardness and Young modulus through nano-indentation tests. Material used in this study is S 235 JR structural steel.

3. Results and Discussions

Circular specimens fabricated from S 235 JR are subjected to combined loadings. Initial loading sequence consists in of applying gradual extensions through tensile test. Than specimens are elastic recovered. Finally, the subsequent loading sequence is torsion. For surface failure analysis images were taken of the

specimen center by SEM technique at different magnifications (magnitudes ranging from 50X to 1000X). In Fig. 1 is represented specimen location were micrographs are made.

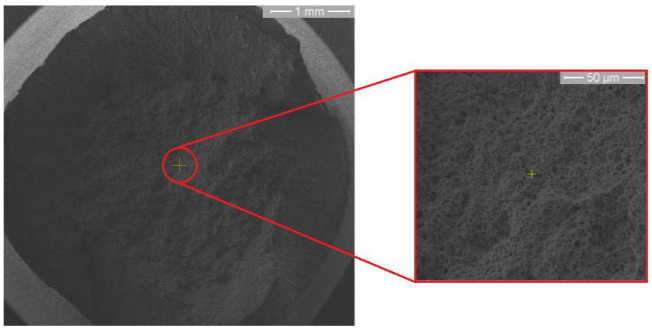

Fig. 1 – Location of micrographs (for all resultant fracture surfaces).

By varying level of extension applied by initial tension different twist angles are necessary to break each specimen. In Fig. 1 is presented a surface failure from a specimen subjected to uniaxial tension test, were necking is present.

In Fig. 2 are illustrated failure modes for three different fracture surfaces corresponding to specimens S_A, S_ C and S_F.

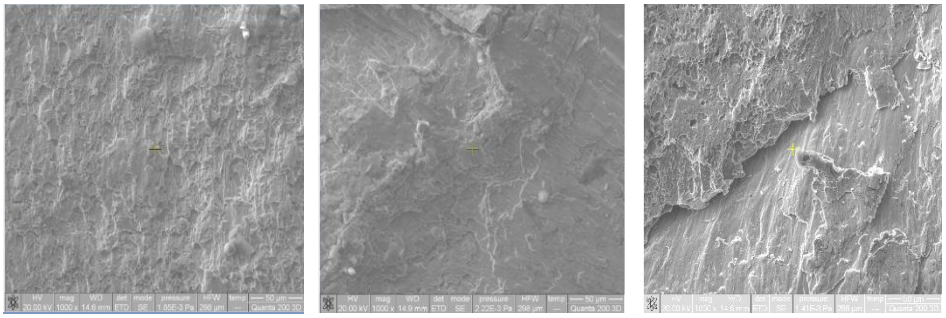

S_A *S_C* *S_F*

Fig. 2 – SEM fractographs for three specimens showing failure mode (1000X).

S_A is the specimen with the highest value of extension and the smallest value of twist angle. Although twist angle value was small it can be observed the influence of subsequent torsion test. Increasing twist angle value for each specimen the influence grows resulting failure modes like in Fig. 2 (S_C and S_F).

Instrumented indentations tests are made in 9 indentation points, on two perpendicular radial direction (Fig. 3) upon disc samples extracted from fractured circular specimens.

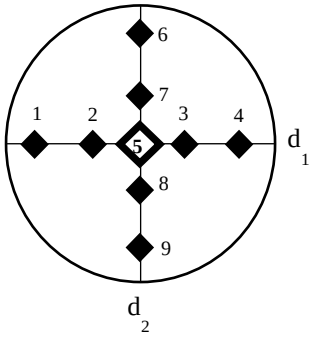

Fig. 3 – Distribution of points where nano-indentation tests were performed on disc samples.

To capture the variation of hardness and Young's modulus on the disc have been traced two perpendicular directions (d_1 and d_2). The point of intersection of the two is the center piece (point 5). Medium values of hardness and Young's modulus for each sample are considered to be representative in illustrating their evolutions.

In Fig. 4 is presented the variation of Young's modulus for six disc pieces cuted form circular specimens.

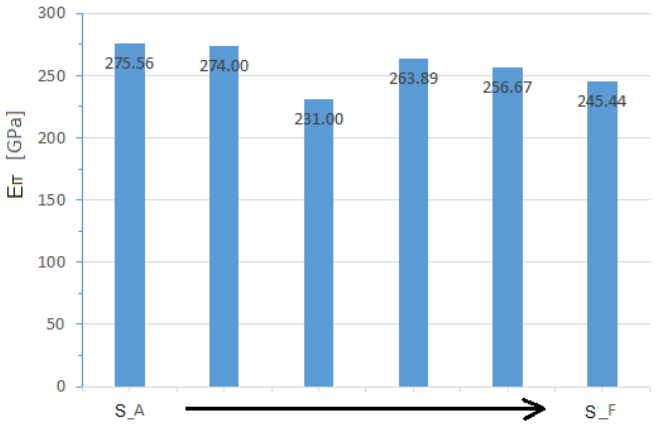

Fig. 4 – Variation of Young's modulus.

Can be observed that maximum values are registered for samples S_A (275.56 GPa) and S_B (274 GPa) and the lowest values are find for S_C (231 GPa) and S_F (245.44 GPa).

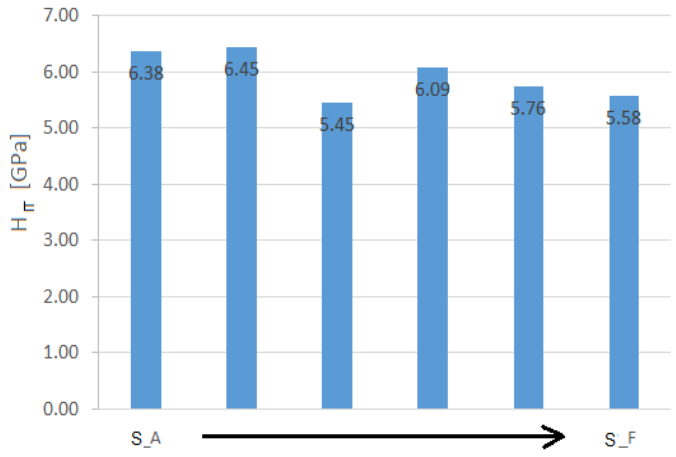

Fig. 5 – Evolution of hardness.

It was found that the higher hardness values (6.38 and 6.45 GPa) are associated with test pieces that have had high levels of extensions applied by initial tensile test (S_B and S_A from Fig. 5). Distribution of the two parameters is not uniform on the perpendicular directions, with higher values outside the disc and lower values inside.

4. Conclusions

This study investigates the influence of complex loading paths on material behavior at microscopic level. Subsequent torsion tests has a major influence on samples final failure previously subjected to tension tests. Hardness and Young modulus, obtained through instrumented indentation tests shows that, excepting sample P_3, they decrease when the level of extension applied by initial tensile test is reduced. Microstructure has a preferred orientation induced by torsion subsequent test. Through the combined loadings can be estimated limit values for the two different stresses (normal and tangential), before material final failure occurs.

REFERENCES

Andrușcă L. *et al*., *Design of a Testing Device for Cruciform Specimens Subjected to Planar Biaxial Tension,* Applied Mechanics and Materials, **809-810**, 700-705 (2015a).

Andrușcă L. *et al*., *Investigation of Materials Behavior under Combined Loading Conditions,* Bul. Inst. Polit. Iași, **LXI (LXV)**, *2* (2015b).

Barsoum I. *et al*., *Rupture Mechanisms in Combined Tension and Shear -Micromechanics,* International Journal of Solids and Structures **44**, 5481-5498 (2007).

Barsoum I. *et al*., *Micromechanical Analysis on the Influence of the Lode Parameter on Void Growth and Coalescence*, International Journal of Solids and Structures, **48**, 925-938 (2011).

Graham S. *et al*., *Development of a Combined Tension–Torsion Experiment for Calibration of Ductile Fracture Models under Conditions of Low Triaxiality*, International Journal of Mechanical Sciences, **54**, 172-181 (2012).

Haltom S.S. *et al*., *Ductile Failure under Combined Shear and Tension*, International Journal of Solids and Structures, **50**, 1507-1522 (2013).

Hu G. *et al*., *Yield Surfaces and Plastic Flow of 45 Steel under Tension-Torsion Loading Paths*, Acta Mechanica Solida Sinica, 25 (2012).

Khoddam S. *et al*., *Surface Wrinkling of the Twinning Induced Plasticity Steel During the Tensile and Torsion*, Journal Materials and Design, **60**, 146-152 (2014).

Li J. *et al*., *Micro-Structural Evolution Subjected to Combined Tension–Torsion Deformation for Pure Copper*, Materials Science & Engineering A, **610**, 181-187 (2014).

Wang C. *et al*., *Microstructure Evolution, Hardening and Thermal Behavior of Commercially Pure Copper Subjected to Torsion Deformation*, Materials Science & Engineering A, **598**, 7-14 (2014).

*** ISO 14577-1, *Metallic Materials — Instrumented Indentation Test for Hardness and Materials Parameters* (2002).

CARACTERIZAREA EXPERIMENTALĂ A MATERIALELOR SUPUSE LA SOLICITĂRI COMBINATE PART I: TRACŢIUNE CU TORSIUNE

(Rezumat)

Această lucrare prezintă studiul evoluţiei microstructurii şi a unor caracteristici ale materialelor supuse la solicitări combinate (tracţiune şi torsiune). Şase epruvete cu secţiune circulară, confecţionate din oţelul structural S235 JR, au fost supuse la un ciclu de testare ce a constat din trei faze - o solicitare iniţială în domeniul elasto-plastic, revenire elastică şi o solicitare subsecventă până la rupere. Testele s-au realizat după cum urmează: iniţial, epruvetele au fost solicitate la tracţiune cu diferite valori ale extensiei, iar subsecvent au fost solicitate la torsiune, până la rupere. Suprafeţele de rupere ale epruvetelor au fost analizate microscopic prin tehnica SEM. Din epruvetele rupte au fost prelevate probe sub formă de disc, pe care s-au efectuat teste de indentare instrumentate. Prin aceste teste s-au determintat valorile durităţii şi modulului Young. S-a constatat că cei doi parametri au o tendinţă descrescătoare, începând cu epruveta care a fost cel mai mult solicitată la tracţiune şi cel mai puţin la torsiune, P_A şi terminând cu epruveta P_F. Suprafeţele de rupere rezultante în urma solicitării combinate arată că influenţa semnificativă asupra microstructurii materialului o are solicitarea subsecventă la torsiune. Se observă o orientare preferenţială a grăunţilor, ghidată de solicitarea la răsucire. Prin solicitarea combinată la tracţiune cu torsiune, se poate aprecia influenţa tensiunilor normale şi tangenţiale asupra cedării materialelor, în vederea estimării valorilor limită corespunzătoare fiecăreia dintre cele două solicitări.